論文 / 著書情報
Article / Book Information

題目(和文)	
Title(English)	An investigation on the muscle synergy model into signal source and muscle type discrimination through hand motion estimation
著者(和文)	KimYeong Dae
Author(English)	Yeongdae Kim
出典(和文)	学位:博士(学術), 学位授与機関:東京工業大学, 報告番号:甲第12019号, 授与年月日:2021年3月26日, 学位の種別:課程博士, 審査員:小池 康晴,金子 寛彦,八木 透,長谷川 晶一,吉村 奈津江
Citation(English)	Degree:Doctor (Academic), Conferring organization: Tokyo Institute of Technology, Report number:甲第12019号, Conferred date:2021/3/26, Degree Type:Course doctor, Examiner:,,,,
学位種別(和文)	博士論文
Type(English)	Doctoral Thesis

Tokyo Institute of Technology

Graduate major in Human Centered Science and Biomedical Engineering

Department of Information and Communications Engineering

An investigation on the muscle synergy model into signal source and muscle type discrimination through hand motion estimation

Yeongdae Kim

Submitted in partial fulfillment of the requirements for the degree of

Doctor of Philosophy (Ph.D.)

Contents

Abstract

Electromyography (EMG) in the human-computer interface is one of the competent input signals. Its intuitive applicability with the same strategy of the body movements fits prosthesis and virtual reality interface applications. The advancement of EMG signal processing facilitated identifying postural pattern or locomotion trajectory estimation, but not together. The existing estimation models are usually either discrete classification of complex motions or regression of a single joint. However, the complex regression model is elusive because of the crosstalk inherent in EMG signals. Signal source decomposition demands for a complex movement estimation with continuity. Among famous decompositions are the non-negative factorization and independent component analysis, which are also algorithms to compute muscle synergy. This study explores the muscle synergy-based EMG signal decompositions and investigates the validity of muscle synergy in movement and muscle type discrimination. First, multi-degree hand movements containing combined two-dimensional wrist movements and grasping were discriminated then linearly regressed using muscle synergy. Its estimation performance was compared with the existing musculoskeletal model in γ correlation and normalized error. Comparing linear regression performance from muscle synergy with the musculoskeletal model confirmed the robustness of muscle synergy in movement estimation and movement type discrimination. Finger movement estimation in the two-elbow posture was conducted after hand motion estimation to explores the crosstalk between the superficial and deep muscles with high-density EMGs on the forearm. The sequential EMG decompositions by muscle synergy onto the multi-channel EMG surrounding the entire forearm enabled deep muscle identification with equivalent signal fidelity of superficial muscles, and this drastically improved finger movement estimation. In addition, stepwise change of muscle signals revealed the role of decomposition algorithms. The muscle synergy proposed in this study gives either robust or improved signal fidelity input signals that could expand to the existing EMG based human-machine interface.

Chapter 1 Introduction

In the 21st century, the emerging technology of 3D display such as head mount display gives anticipation of augmented/virtual reality. New technologies demand interfaces that can keep up with their functions, as mouse/keyboard interface has been matched with graphic visualization of the computer. To fit into the new era, collaborative new interface devices and algorithms are vigorously studied, aiming for user-friendly features. Electromyography (EMG)-based interface is one of the candidates.

This study deals with EMG based interface regarding wrist and hand movements using forearm muscles. The hand is a highly dexterous instrument in the human body that has abundant adaptability to numerous functions. Therefore, in augmented/virtual reality, hand motion is one of the most effective tools to express the intention of the users. Also, the application of an EMG-based interface could span the rehabilitation and prosthesis. The loss of hand functions makes daily living difficult such as wearing, eating like fundamental and natural behaviors. Hand motion estimation using EMG has been studied by several researchers from the 90s to the present. From implementing the physical parameters of the body to simply utilizing machine learning for classification, various EMG analysis showed high-precision movement in many procedures.

In real use, however, there still exist several issues to overcome. Dexterous hand motion generates from several muscle fibers inside the forearm. However, the detection of individual muscle activity using surface EMG is a controversial issue, sometimes regarded as physically impossible. The muscles on the forearm are layered one over another. This physical location brings about crosstalk and makes a small number of EMG signal analysis to be hard to identify the specific target muscle activities in complex

movements so that further signal processing is demanding. This study deals with such signal processing issue with scientific concept ‘muscle synergy’ in engineering technique and try to figure out signal sources and applied the information into the interface.

1.1 EMG

Electromyography (EMG) records the bioelectric activity in the muscle representing voluntary contraction. Motor neurons in the spinal cord and the brain give commands, and the contraction occurs in multiple motor units inside muscles. Vibrating EMG signals originate from the superposition of such a massive number of the motor unit action potential. EMG-driven parameters such as Integrated EMG, Zero Crossing, and quasi-tension of selected muscles enable researchers to estimate muscle activities and even body movements (Phinyomark, et al., 2018). Figure 1.1 shows the EMG signals activation with subsequent Quasi-tension with the process of rectification.

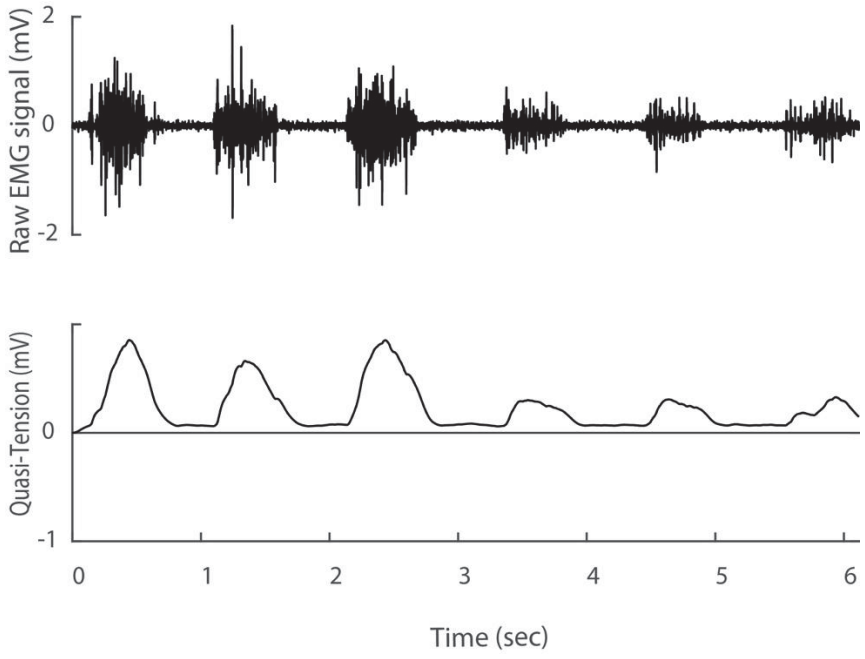

Figure 1.1 Time Series EMG signal (Up) and subsequent Quasi-tension (Down)

This control technology is applicable for not only exoskeletal devices of amputee and paralyzed patients but also a wide range of applications for augmented/virtual reality. One of the primary advantages of EMG is that it predicts movements using signals from the central nervous system that control the body so that the cost of users learning the EMG interface is small. If surface EMGs can detect each muscle activity, we can see and generate diverse body movements.

1.2 Muscle Synergy

Muscle synergy is defined as a group of muscle activations recruited by a neural command (Torres-Oviedo, et al., 2006). The existence of this phenomenon was proposed by Nikolai Bernstein (Bernstein, 1967) as a neural strategy simplifying the musculoskeletal model that it is too complex to the high degree of freedoms (DOFs). Studies on frogs have proposed that a complex repertoire of movements can emerge from the appropriate control and selection out of few synergies which respectively represent a primitive movement (Tresch, et al., 1999). Ting & McKay (2007) also proposed that the nervous system uses muscle synergies as a set of heuristic solutions to transform task-level goals into detailed spatiotemporal patterns of muscle activation (Figure 1.2).

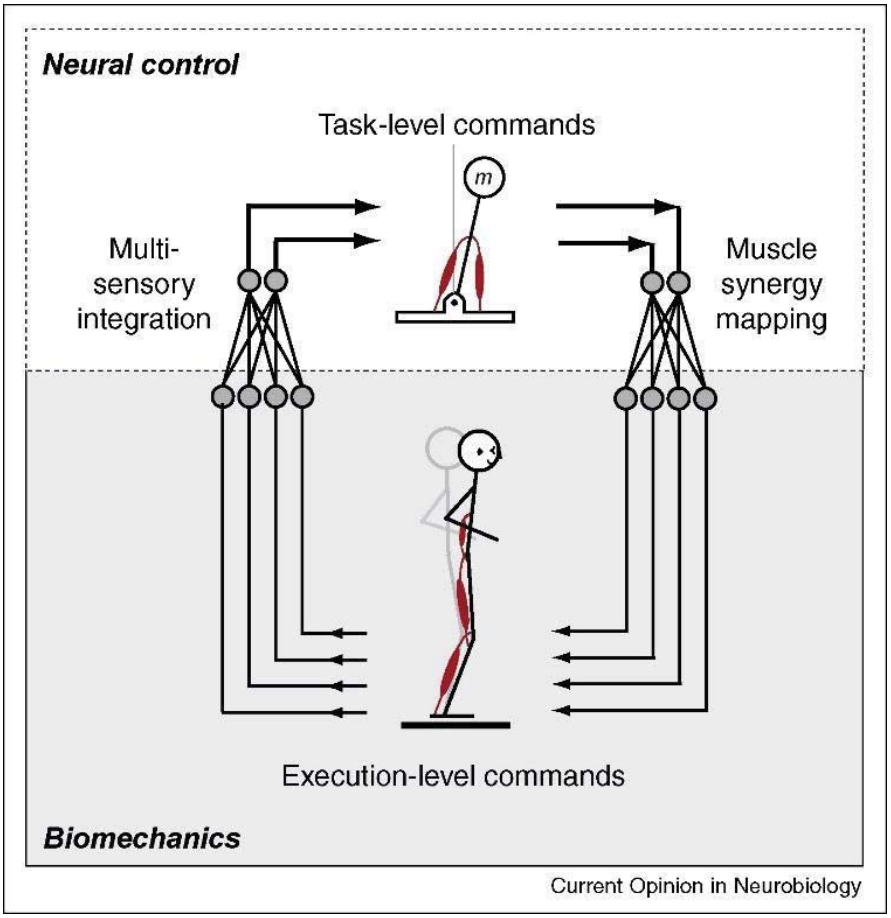

Figure 1.2 Muscle synergies allow task-level neural commands to be translated into execution-level muscle activation patterns. This hierarchical structure mirrors that of multisensory integration systems. ©Reprinted from Current Opinion in Neurobiology, Vol 17, Ting & McKay, Neuromechanics of muscle synergies for posture and movement, 622-628, Copyright (2007), **with permission from Elsevier**

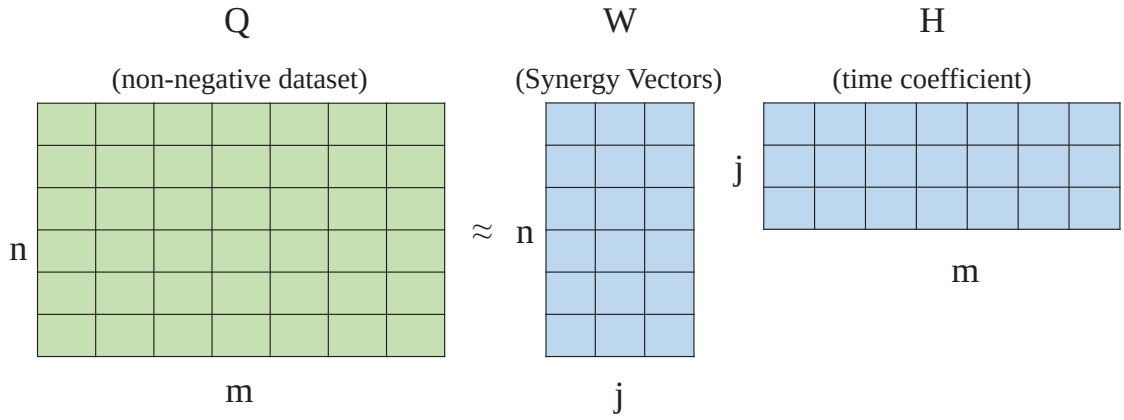

Figure 1.3 Brief overview of non-negative matrix factorization

Muscle synergy derivation was mainly conducted using Non-negative matrix factorization (NMF) as shown in Figure 1.3. NMF is one of the main blind source separation (BSS) techniques to solve the following problem.

$$\boldsymbol{Q} \cong \boldsymbol{WH} \tag{1}$$

where Q is the muscle signals in a non-negative $n \times m$matrix with n being the number of EMG channels, m being the number of samples;$W = [\mathrm{w}_1, \dots, \mathrm{w}_\mathrm{j}]$is the synergy vector series in n by j matrix, wherein j is the independent variable that defines the number of synergies and $w_1 = [c_1, \dots, c_n]^T$ representing a single set of synergy; H is time coefficient the synergy in j by m matrix. NMF optimizes the synergy and time coefficient vector based on the square of the Euclidean distance and other parameters (such as divergence) (Lee & Seung, 2001). In the case of the method of reducing Euclidean distance, the update rules are shown below with $\boldsymbol{W_k}$, $\boldsymbol{H_k}$ are the k-th iteration results of update rules.

$$\boldsymbol{W_{k+1}} \leftarrow \boldsymbol{W_k} + \frac{(\boldsymbol{QH^T - WHH^T})_k}{\boldsymbol{H_k H_k^T}} \tag{2}$$

$$\boldsymbol{H_{k+1}^T} \leftarrow \boldsymbol{H_k^T} + \frac{(\boldsymbol{Q^T W - H^T W^T W})_k}{\boldsymbol{W_k^T W_k}} \tag{3}$$

Chapter 2 Backgrounds and Aim

2.1 EMG Preprocessing

The surface EMG signal contains various noise and artifacts from physical contamination such as power source noise, movement, skin/electrode impedance artifact. And even the small-amplitude spikes induced by static electricity or random nature could be the source of noise components from the environment (Chowdhury, et al., 2013). The inherent noises such as blood flow in the muscles, muscle fiber composition, and distance between muscle fibers could be another source of the noise components. For this reason, EMG preprocessing is an essential step in the EMG analysis.

- Bandpass filtering

The SENIAM project and the International Electromyography and Exercise Science Association (ISEK) gave scientific recommendations to use bandpass filters (10 - 500 Hz) under 1 kHz sampling rate to reduce the aliasing effect.

- Linear envelope

Linear envelope is a combination signal processing that comprise rectification and low pass filtering on the EMG signals. The high-frequency region of the EMG signal reflects individual motor unit action potential, and low frequency reflects the firing rate of α motor neurons (Koike & Kawato, 1995). Thereby linear envelope (quasi-tension) makes EMG signal to be highly correlated with joint torque of the muscle.

- Normalization

The optimal condition of EMG normalization is matching the EMG activation according to a specific force level so that it connects EMG signals to the force unit. However, when it is not applicable, there are different methods to be applied (Halaki & Ginn, 2012)

a. maximum(peak) activation levels during maximum contractions.

(= Maximum voluntary contraction (MVC))

MVC is one of the most common methods of EMG normalization. Though the reference tests are not fixed per muscle, stimulations of all involved muscle parts are particularly important. Participants could distort normalization parameters by using the wrong muscle in the designated muscle contraction trial sets. Thereby, MVC in the isometric condition is preferable but if the condition is not matching, the dynamic contraction would be better than the following method.

b. Peak or mean activation levels obtained during the task under investigation

In some cases, normalization is performed using the maximum value of all data so that the data after the normalization process does not exceed 1. However, in this case, real-time analysis becomes impossible and normalization becomes task-dependent, making comparison with other tasks impossible. Nevertheless, this normalization method may be useful when high intensity exercise is unavailable as in patients.

2.2 EMG-based Hand Motion Estimation

There are many studies conducting hand motion estimation using EMG. The followings are some examples within a year.

Mukhopadhyay & Samui (2020) classified eight different hand movements, that are six wrist joint movements and hand grip and opening from seven EMG electrodes using feed-forward Deep Neural Network (DNN) model and compared with the existing machine learning tools. Their DNN model achieved comparable performance with SVM, with minimal processing in feature selection.

Simão et al. (2019) propose the use of recurrent neural networks (RNNs) to improve the online classification of hand gestures using two Myo armbands (Thalmic lab, USA) placed on the forearm muscles, they showed equivalent performance with existing machine learning in less time cost.

Ameri et al. (2019) tested RNN in eight bipolar EMG channels in four type of movements and their combinations. Their model showed more than ninety percent accuracy on the flexion, extension, pronation, supination movements and their combinations even with different width and distance.

As illustrated, many researchers conducted hand motion estimation using each of their own machine learning model. However, their focus was mainly on the feasibility of machine learning on the bio-signal. For this reason, their target movements are limited to single joint movements even for measuring wrist joint muscles.

2.3 Muscle Synergy

Some of the latest studies on muscle synergy employed in human machine interface are reviewed in this section.

Shima & Tsuji (2010) proposed a pattern classification for user motions to create input signals for human-machine interfaces from electromyograms (EMGs). This method is implemented to represent combinations of simple motions using a recurrent neural network by combining synergy patterns of EMG signals preprocessed by the network (Shima & Tsuji, 2010). The results showed that 18 motions (12 combined and 6 single) were classified with learning on 6 single motions (average rate: 89.2 ± 6.3%), and the amputee participant controlled a prosthetic hand both on single and combined motions.

Based on multiple days' study by Ison and Artemiadis (2015), new muscle synergy space naturally emerges as participants identify the system dynamics of a myoelectric interface. These synergies correlate with long-term learning, increasing performance over consecutive days. Synergies were maintained after one week, helping participants retain efficient control and generalize performance to new tasks. The extension to robot control was also demonstrated with a robot arm performing reach-to-grasp tasks in a plane. The ability to enhance, retain, and generalize control, without a need to recalibrate or retrain the system, supports control schemes promoting synergy development, not necessarily user-specific decoders trained on a subset of existing synergies, for efficient myoelectric interfaces designed for long-term use. The study supports a shift in myoelectric control schemes toward simultaneous proportional controls learned through the development of unique muscle synergies.

Antuvan *et al.* (2016) compared the performance of a decoder trained using extreme learning machine (ELM) for two different features (EMG and synergy) which are for the myoelectric-based interface which is able to identify and online classify, upper limb motions involving shoulder and elbow. The performance of the decoder was tested in online motion control by using a simulated graphical user interface replicating the human limb: participants are requested to control a virtual arm by using their muscular activity. The decoder performance was quantified using ad-hoc metrics based on motion selection time, motion completion time, and classification accuracy. The work demonstrated the better robustness of online decoding of upper-limb motions and motor intentions when using the synergy feature.

In muscles synergy studies, the tasks approached the actual movement on the daily life such as combination of reaching/grasping.

2.4 Purpose of The Study

The purpose of the study is to enable multi joint complex hand motion estimation. To do this, we need to find out the activation of each of the various muscles stacked in layers. This will span the application region and, in the end, enable the natural movement. I consider EMG sensor signal as a mixture signals composed of multiple muscle signals and noise components. Therefore, signal discrimination is necessary before inserting to system models. For this, the muscle synergy concept gets used with NMF as the BSS method. Besides, I suppose that through signal analysis such as NMF from these signals, we will be able to obtain specific muscle signals or primitive neural commands that cause movement. The following experiment tested whether muscle synergy could discriminate neural command and muscle activities from control tasks.

Chapter 3 Muscle Synergy-based Hand Motion Estimation

3.1 Introduction

Chapter 3 tested the feasibility of the muscle synergy model by comparing the performance with an existing model. As mentioned in the previous chapters, surface electromyography (EMG) signal-based models, algorithms, and numerous techniques have arisen for prosthesis controls and clinical controllers. Although it was a discreet way, several studies had attempted and shown their control method in prosthetic machines (Nishikawa, et al., 1999), virtual hands (Sebelius, et al., 2005), and exoskeletons (Khokhar, et al., 2010) using hand gestures and wrist motions. Their control algorithms were as diverse as their control targets. They used machine learning (Nishikawa, et al., 1999), feed-forward neural network (Kita, et al., 2006), and other linear classifiers (e.g., k-NN and Bayes).

Previous studies obtained high performance for movement but received a rigorous evaluation from real users (Biddiss, 2009). They demanded various and natural motions necessary for daily life, which naturally led to studies based on continuous estimation. Castellini & van der Smagt (2009) classified grasping type and estimated its force regression with a support vector machine. Another force estimation study showed promise of applicability to unilateral amputees by employing a bilateral mirror-training strategy (Nielsen, et al., 2010). In movement estimation, Artemiadis & Kyriakopoulos (2010) tried the shoulder and elbow joints of four rotational degree-of-freedoms (DOFs) model. Jiang et al (2012) even suggested an algorithm of the three DOFs of the wrist for simultaneous estimation; However, these continuous estimations did not step on the complex estimations of the wrist joint movements and gripping.

If I have to pick the biggest issue for complex movement estimation, it would be the crosstalk. Wrist joint and finger muscles placements are adjacent inside the forearm. Therefore, surface EMG sensor extract not only the target muscle signal but also the adjacent signals derived from neighboring muscles. In this regard, some researchers used sensor attachment in the way of suppressing inclusion between each muscle, and then considered each sensor signal as a target muscle signal and conducted the analysis. In this chapter, my sensor positions keep the previous research rules while treating the sensor signals as a mixture of multiple muscle signals. Movement estimation performs both on the gripping force and wrist joint movements by separating the crosstalk between different signal source using muscle synergies.

The idea of synergy-based estimation has a root in the following studies. Muscle synergy is regarded as a neural command (Torres-Oviedo, et al., 2006). And combinations of muscle synergies generate from individual motion can make complex movements under pattern recognition (Tresch et al., 1999; Shima & Tsuji, 2010). Then we shall test whether the movements can be estimated in time series using the combination of the synergies.

Chapter 3 tests the feasibility of the muscle synergy model by comparing the performance with an existing model. The analysis compared the muscle synergy model with the musculoskeletal model (MSM) the complex motion estimation performance. Specifically. A second-order computational motor control model with nonlinear dynamics. The MSM showed high performance in a one-degree-of-freedom joint angle for flexion and extension by computing muscle elasticity and viscosity (Kambara, et al., 2013). Kawase et al. (2017) even developed a simplified computational model that investigated the estimation of three different joint angles (i.e., elbow, wrist, and finger).

He addressed that there was little influence between finger joint and wrist position estimation. Therefore, this experiment tests whether the muscle synergy model shows the equivalent or more robust estimation performance under complex motion between gripping and wrist joint movements.

3.2 Wrist Motion and Synergy Preferred Direction

Before the main tasks, a preliminary test was conducted on muscle synergy-based wrist joint angle estimation on two participants (males, aged 26 and 44, right-handed) to check whether linear regression is enough for wrist joint angle estimation. For that, EMG sensors from the Trigno™ Wireless system, and a Hand Tracking device based on potentiometer were used. In each trial, the participants followed the ball trajectory at three different speeds on the screen using a hand tracking device. The trajectory and EMG signals of the task were measured. Figure 3.1 shows the preferred direction of four wrist synergies from the preliminary trial, and Figure 3.2 shows the regression performance in two wrist joint angles. The average correlation coefficient on the wrist joint angles was more than 0.7 in two participants (0.735 in minimum).

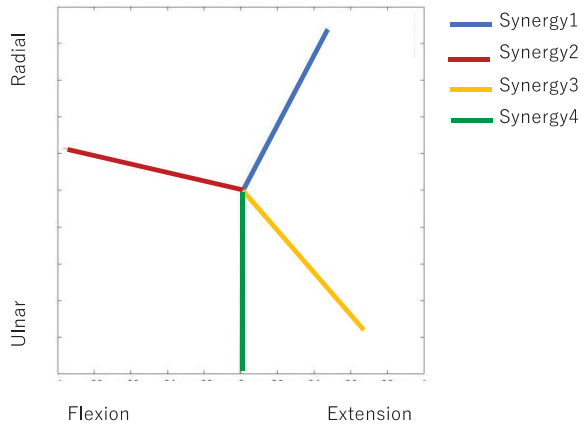

Figure 3.1 Preferred direction of synergy in preliminary hand tracking trials.

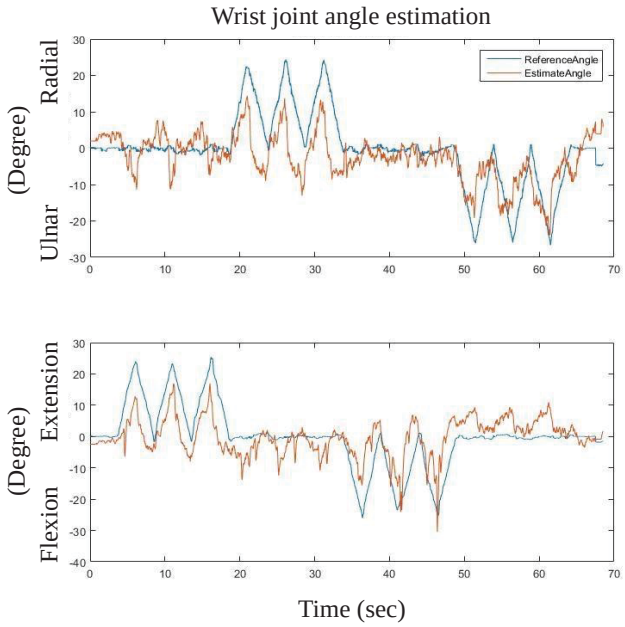

Figure 3.2 Horizontal(flexion/extension) and vertical (Radial/Ulnar deviation) wrist joint angle estimation in preliminary trial.

The synergy computation from preliminary trials showed the distributed synergy to a four-movement direction and regression in flexion/extension, radial/ulnar deviation. It also confirmed the feasibility of vertical and horizontal axis movement estimation. However, the step-tracking movement task got some feedback. Following the trajectory, the participants felt that they need more deliberate control over the wrist motion so that synergy sets could be corrupted by stiffness action to match the ball speed. As a replacement, free-motion tasks without a target were applied in the main experiment.

3.3 Experimental Procedure

Ten healthy participants (males, aged 28.0±5.7, nine right-handed, one left-handed, none ambidextrous) joined the main experiment. No participant had a history of any form of neurological disorder. They got asked to use their dominant hand (either left or right hand) during the experiment.

The experiment protocol was approved by the ethics committee of the Tokyo Institute of Technology (2014042) and was carried out in accordance with the Declaration of Helsinki. Written consent was obtained from each participant before the experiment.

Table 3-1. Forearm muscle with channel number

Muscle Position	
Ch. 1	Extensor Carpi Radialis (ECR)
Ch. 2	Extensor Carpi Ulnaris (ECU)
Ch. 3	Flexor Carpi Ulnaris (FCU)
Ch. 4	Flexor Carpi Radialis (FCR)
Ch. 5	Abductor Pollicis Longus (APL)
Ch. 6	Flexor Digitorum Superficialis (FDS)
Ch. 7	Flexor Digitorum Profundus (FDP)

Table 3-1 indicates the wrist and grip muscle groups chosen on the experiment. Five muscles are wrist joint muscles (i.e., ECR, ECU, FCU, FCR, and APL) and two are grip muscles (i.e., FDS and FDP). Several wrist-joint experiments analyzed four wrist muscles (i.e., ECR, ECU, FCU, and FCR) (Kawase et al., 2017; Lee et al., 2015), which are the flexor and extensor muscles of the wrist with different deviations (Radial and Ulnar). My experiment added APL, an extensor of the thumb, to trace the radial movement of the wrist. The FDS and FDP—the flexor muscles of the finger—are chosen to estimate the grip force with a synergy-based model. Figure 3.3 shows the placement of the EMG sensors on the forearm. The EMG sensor equipment is Trigno™ EMG system.

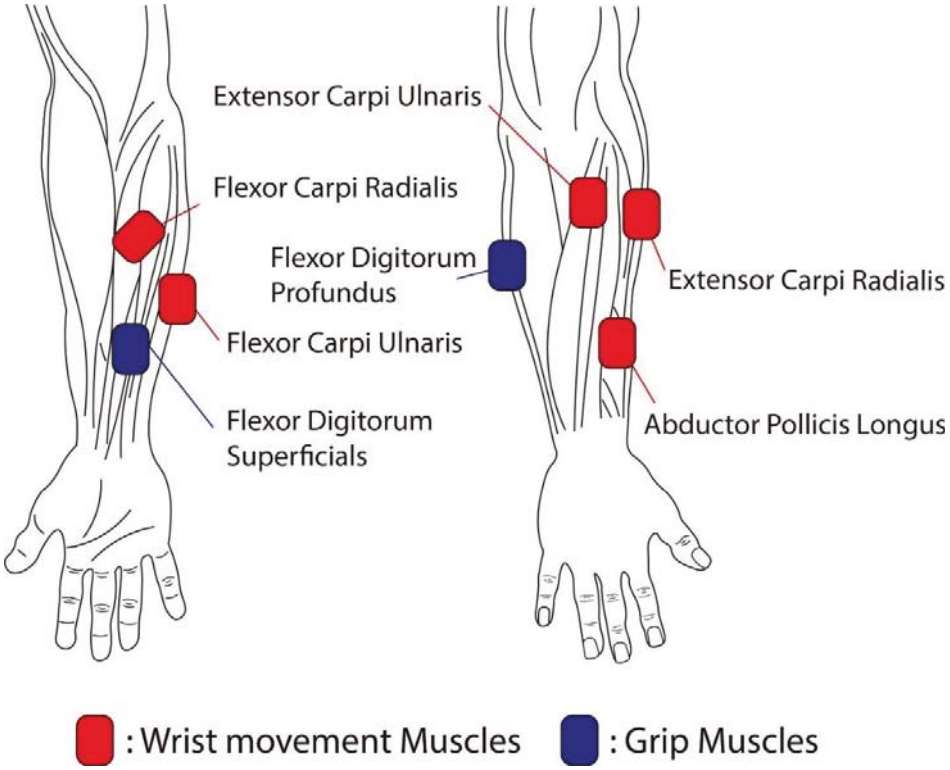

Figure 3.3 Seven EMG channel placements on five wrist joint-related muscles (red-colored) and two grip muscles (blue-colored)

Participants took two sessions. The first task focused on a wrist motion, measuring the EMG signals and wrist joint angles in different movement conditions. The second task focused on a grip force, measuring the EMG signals and grip forces in different grip force levels. Thus, the experiment and the analysis were divided into two sessions, one checking the wrist movement at a certain grip condition and the other checking grip force at a certain posture.

In the first task, Trigno™ EMG system measured EMG signals and wrist joint angles using the ordinary (EMG) and IM (wrist joint angles) sensors of the system. Figure 3.4 shows the placement of the two IM sensors. One was were attached to the back of the hand and the other to the back of the forearm; they were to detect the relative wrist joint angle from the forearm.

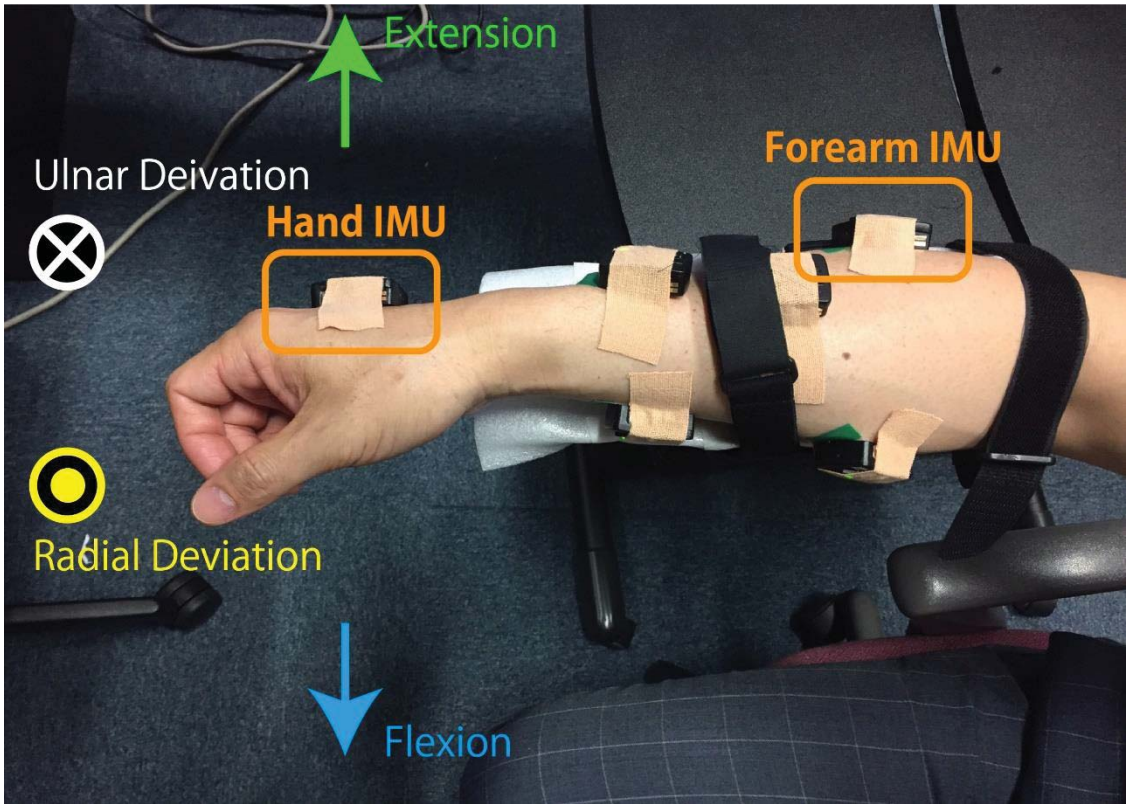

Figure 3.4 First task: experimental posture in the center-position and movement direction with the placement of the IMU sensors. Yellow-colored rectangles emphasize the positions of the IMU sensors placed at the back of the hand and forearm.

Participants placed their forearms on the table fastened by a wrist binder and reached out of the table. From then, they performed four wrist motions: flexion, extension, and radial/ulnar deviation in two different conditions. They conducted wrist motion with and without gripping. Wrist motions also had three criteria in movement range. According to the participant's comfort level, they carry out comfortable maximum limit (with and without grip), half of the comfortable maximum limit (without grip only), and stiffened movement with force exertion (without grip only). Each condition consists of three trials requiring each trial to conduct three times for each motion. Then, the gripping action

(without wrist motion) began in the center-position (Figure 2) when the participants performed strong and weak grips three times each.

In the second task, the Trigno™ EMG system measured EMG, and the ReachMAN robot (Yeong, et al., 2009) measured grip force. Participants adjusted the angle of the grip handle to their best fit while maintaining a center-position posture. In this task, three levels of grip strength get performed: strongest, half, and a quarter of gripping power. The strongest grip force (in newton N) varied for every participant with an average of 16.2 ± 3.2 N.

3.4 Data Acquisition and Preprocessing

The sampling rate differs per data. The EMG sampling rate is 2kHz, IMU wrist angle is 74Hz, and ReachMAN force sensor is 100Hz. Lab streaming layer (LSL) in MATLAB 2018b program (Kothe, 2014) collects all data with corresponding timestamps so that the timing of each data is aligned using the timestamps.

The seven-channel EMG signals processed bandpass filtering and linear envelop before synergy computation. In normalization, the MVC method implemented using the combined hand motion tasks, co-activating both grip and wrist motions trial.

Regarding wrist motion data, there applied Madgwick IMU algorithm to estimate the two-dimensional wrist joint angle (Madgwick, 2010). IMU sensors were placed on the back of the hand and forearm in a straight line when the wrist joint is at zero-degree to track the orientational difference between the hand and forearm.

Participants performed self-paced movements without visual feedback; consequently, most of them performed diagonal movements even if the instruction was

only vertical and horizontal directions. To take this into account, the two angles obtained by the IMU algorithm were normalized by each angle's absolute maximum value; the sum and difference obtained can be seen in Figure 3.5. The resultant angle reference was applied in all the following models.

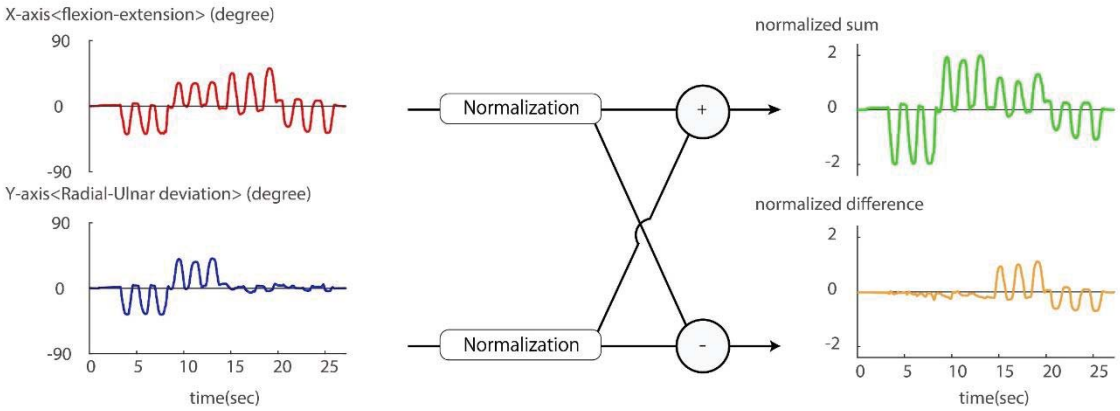

Figure 3.5 X-axis stands for flexion-extension dimension while Y-axis stands for radial-ulnar deviation. To compensate for the inclined diagonal movement of participants in self-paced movement, two angles were normalized, and their sum and difference were subsequently computed.

3.5 Muscle Synergy Linear Regression and Musculoskeletal Model

A synergy-based linear regression model was used to estimate wrist and grip values. To reduce computational costs in a model calculation, a simplified version of the nonnegative matrix method, i.e., the hierarchical alternating least square (HALS) method, was used (Cichocki & Phan, 2009). Apart from the computational cost, HALS also has a wide capability: it can work with a large number of components (Cichocki & Phan, 2009), in contrast to the canonical NMF method (Lee & Seung, 2001), which is only applicable if the number of the sources is greater than the number of components; Cichocki & Phan (2009) shows pride in their paper that HALS can work in conditions where the number

of components is large. This feature of HALS is appropriate in complex movement estimations. When measuring activities, as the object of movement increases, the form of synergy required may also vary. In some cases, the number of reference synergies may be greater than the measured near-front channel. HALS was selected in consideration of these variables. The HALS decompose the normalized quasi-tension with the same update rules without normalization per repetition.

For complex hand movement estimation, wrist motion synergies and a grip synergy composed a synergy set. Then linear regression performed in wrist angle estimation using wrist motion synergies as input. The reference angles are normalized sum and difference of the wrist angle (flexion-extension, radial-ulnar deviation) θ_i onto equation (4) below:

$$\theta_i = a_{0,i} + a_{j,i}s_j + \cdots + \epsilon \quad (4)$$

Here, $a_{0,i}$ denotes angle bias, $a_{j,i}$s are the regression coefficients for each synergy coefficient s_j, and ϵ denotes random noise error. Synergy set with regression coefficients calculation conducted in two grip motion and wrist motion task separately, and the parameters applied to all other trials.

3.6 Statistical Analysis on Estimation Performance of Computation Models

An exhaustive cross-validation was used to test the performance of each model per participant, with indices used to estimate performance. The following Pearson correlation coefficient (r) and normalized root mean square error (nRMSE) composed the indices

$$r = \frac{\Sigma_{i=1}^{n}(x_i-\bar{x})(y_i-\bar{y})}{\sqrt{\Sigma_{i=1}^{n}(x_i-\bar{x})^2}\sqrt{\Sigma_{i=1}^{n}(y_i-\bar{y})^2}} \quad (5)$$

$$nRMSE = \frac{1}{a}\sqrt{\frac{\Sigma_{i=1}^{n}(x_i-y_i)^2}{n}} \quad (6)$$

where *n* is the number of samples, *y* is a reference, *x* is an estimate, and *a* is defined as the normalization coefficient. A in this nRMSE is 90, the limit of the wrist angle range. All statistical analyses were conducted using the ttest2 function of MATLAB 2018b.

3.7 Results

Task1 – Wrist motion Test

Figure 3.6 shows the time series of the wrist angle in two dimensions. Participants got the instruction to rotate their wrists in four directions (up, down, left, and right). They performed freely at their own pace, moving in a sloping trajectory at different angles. Because of that, both models appear to have the underlying assumption that a participant moved in a diagonal direction even if they performed a gradual movement, as shown in Figure 3.6(C).

Table 3-2 and 3-3 shows the exact performance of Synergy-based linear regression model (SLRM) and MSM in *r* and nRMSE. Wrist motion performances *r* on average are 0.789±0.084 in SLRM and 0.761±0.104 in MSM, implying a statistically significant difference ($p < 0.001$, Student's t-test). Similarly, nRMSE also shows a significant difference between SLRM and MSM ($p < 0.01$, Student's t-test). This trend continued during grip-less wrist motion trials (comfortable maximum limit trial, comfortable half limit trial, and stiffened movement trial).

However, when added grip motion, there was no statistically significant difference in r ($p = 0.761$); however, differences still existed in nRMSE ($p < 0.001$, Student's t-test). The r of the comfortable maximum with grip trials was 0.756±0.063 in SLRM and 0.758±0.088 in MSM, and nRMSE was 0.165±0.0.27 in SLRM and 0.180±0.051 in MSM. Finally, in the grip-trial, where r measurement was inappropriate because the wrist motion in the trial is just an indication of a perturbation; nRMSE of SLRM was 0.146±0.025 and MSM was 0.186±0.077 in nRMSE, implying a statistically significant difference ($p < 0.001$, Student's t-test).

In detail, the r values of the comfortable maximum limit trials were 0.826±0.027 in SLRM and 0.799±0.053 in MSM ($p < 0.001$, Student's t-test); the nRMSE was 0.154±0.018 in SLRM and 0.171±0.034 in MSM ($p < 0.001$, Student's t-test). In comfortable half limit trials, the corresponding values were 0.746±0.073 in SLRM and 0.684±0.102 in MSM when measuring r values ($p < 0.001$, Student's t-test), and the nRMSE was 0.120±0.011 in SLRM and 0.126±0.022 in MSM ($p < 0.01$, Student's t-test). The stiffened movement trials also had the same trend in r values, being 0.844±0.034 in SLRM and 0.814±0.059 in MSM ($p < 0.001$, Student's t-test); and, for nRMSE, being 0.185±0.022 in SLRM and 0.210±0.056 in MSM ($p < 0.001$, Student's t-test).

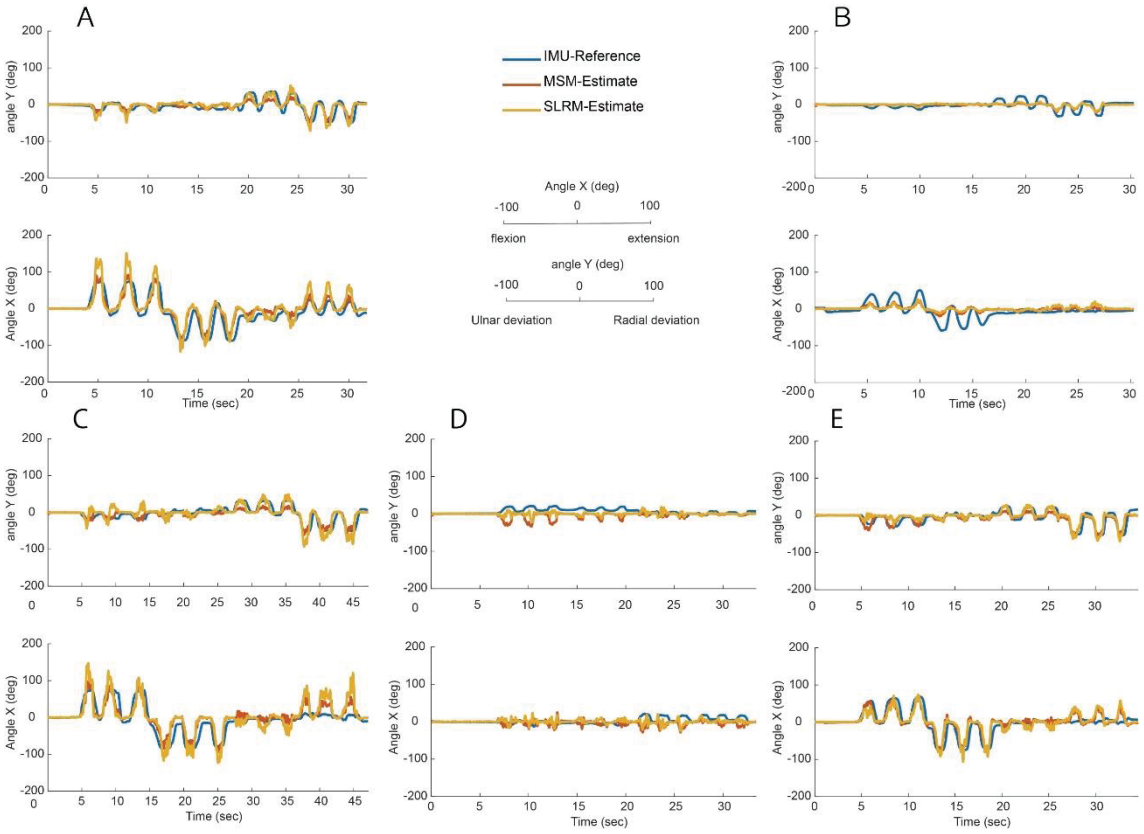

Figure 3.6 2D wrist joint angle estimation in 5 different trials. Angle X corresponds to flexion-extension dimension taking extension as positive. angle Y corresponds to radial-ulnar deviation having radial deviation as positive. The blue-colored line represents the IMU-reference angle derived from two IMU sensors by differentiating relative orientation in Euler angle. The red-colored estimate is a musculoskeletal model (MSM) based estimation having 5 input signals. Yellow-colored estimate stands for synergy-based linear regression model (SLRM)-based estimation deriving synergy derived separately per trial. (A) An example of a comfortable maximum limit trial. (B) an example of half of a comfortable maximum trial. (C) An example of a stiffened movement trial. (D) an example of a grip-trial having twelve times gripping. (E) An example of combined movement of a comfortable maximum limit with grip.

Table 3- 2. MSM performance indicator per participant and trial

Sub	Data type	Comfortable Max		Comfortable half		Stiffened movement		Grip&Motion		Wrist Motion (average)		Grip
		r	nRMSE	*R*	nRMSE	*r*	nRMSE	*r*	nRMSE	*r*	nRMSE	nRMSE
Sub1	***Mean***	0.854	0.154	0.730	0.126	0.882	0.188	0.809	0.174	0.816	0.161	0.129
	SD	0.022	0.017	0.073	0.012	0.016	0.035	0.066	0.032	0.081	0.037	0.021
Sub2	***Mean***	0.853	0.102	0.763	0.072	0.836	0.167	0.730	0.097	0.790	0.110	0.147
	SD	0.027	0.014	0.048	0.010	0.036	0.016	0.181	0.033	0.111	0.043	0.028
Sub3	***Mean***	0.682	0.170	0.556	0.129	0.709	0.208	0.672	0.170	0.652	0.169	0.140
	SD	0.048	0.021	0.104	0.020	0.059	0.032	0.062	0.022	0.097	0.041	0.061
Sub4	***Mean***	0.826	0.211	0.720	0.120	0.818	0.259	0.828	0.182	0.795	0.191	0.098
	SD	0.050	0.037	0.059	0.019	0.060	0.042	0.043	0.024	0.075	0.065	0.059
Sub5	***Mean***	0.816	0.145	0.687	0.109	0.817	0.217	0.750	0.210	0.763	0.173	0.301
	SD	0.084	0.034	0.132	0.016	0.053	0.042	0.060	0.040	0.102	0.058	0.111
Sub6	***Mean***	0.836	0.200	0.686	0.194	0.800	0.261	0.806	0.193	0.777	0.213	0.174
	SD	0.027	0.028	0.103	0.014	0.065	0.035	0.045	0.027	0.093	0.043	0.048
Sub7	***Mean***	0.678	0.224	0.470	0.134	0.699	0.226	0.674	0.179	0.626	0.188	0.506
	SD	0.070	0.021	0.127	0.011	0.109	0.037	0.079	0.024	0.139	0.048	0.180
Sub8	***Mean***	0.808	0.133	0.662	0.110	0.848	0.152	0.754	0.158	0.764	0.139	0.431
	SD	0.061	0.028	0.099	0.015	0.041	0.021	0.047	0.029	0.107	0.033	0.078
Sub9	***Mean***	0.869	0.182	0.864	0.126	0.881	0.180	0.854	0.155	0.867	0.159	0.321
	SD	0.044	0.030	0.042	0.010	0.026	0.023	0.041	0.021	0.043	0.032	0.170
Sub10	***Mean***	0.773	0.192	0.709	0.136	0.852	0.239	0.702	0.284	0.758	0.215	0.175
	SD	0.030	0.050	0.093	0.044	0.036	0.104	0.109	0.106	0.106	0.101	0.082
Mean	***Mean***	0.799	0.171	0.684	0.126	0.814	0.210	0.758	0.180	0.761	0.172	0.186
	SD	0.053	0.034	0.102	0.022	0.059	0.056	0.088	0.051	0.104	0.057	0.077

Table 3-3. SLRM performance indicator per participant and trial

Sub	Data type	Comfortable Max		Comfortable half		Stiffened movement		Grip & Motion		Wrist Motion (average)		Grip
		r	nRMSE	*r*	nRMSE	*r*	nRMSE	*r*	nRMSE	*r*	nRMSE	nRMSE
Sub1	***Mean***	0.885	0.137	0.785	0.116	0.862	0.174	0.863	0.131	0.845	0.140	0.112
	SD	0.017	0.014	0.051	0.012	0.027	0.029	0.021	0.016	0.053	0.030	0.016
Sub2	***Mean***	0.887	0.093	0.780	0.064	0.878	0.143	0.786	0.083	0.828	0.096	0.121
	SD	0.020	0.015	0.025	0.007	0.039	0.017	0.117	0.018	0.087	0.034	0.010
Sub3	***Mean***	0.664	0.166	0.504	0.121	0.775	0.170	0.457	0.175	0.594	0.157	0.062
	SD	0.022	0.013	0.087	0.010	0.029	0.010	0.069	0.013	0.146	0.027	0.009
Sub4	***Mean***	0.843	0.186	0.737	0.136	0.846	0.209	0.776	0.177	0.797	0.176	0.116
	SD	0.018	0.018	0.066	0.017	0.021	0.024	0.031	0.010	0.065	0.034	0.019
Sub5	***Mean***	0.837	0.144	0.770	0.100	0.832	0.239	0.760	0.240	0.796	0.184	0.089
	SD	0.029	0.017	0.034	0.007	0.038	0.024	0.047	0.043	0.060	0.073	0.019
Sub6	***Mean***	0.823	0.200	0.748	0.194	0.855	0.212	0.836	0.178	0.815	0.196	0.224
	SD	0.027	0.018	0.085	0.007	0.023	0.016	0.022	0.017	0.067	0.022	0.043
Sub7	***Mean***	0.801	0.162	0.716	0.133	0.796	0.177	0.639	0.176	0.732	0.162	0.165
	SD	0.026	0.007	0.137	0.008	0.045	0.018	0.100	0.025	0.114	0.027	0.029
Sub8	***Mean***	0.857	0.116	0.821	0.087	0.857	0.152	0.796	0.147	0.831	0.127	0.288
	SD	0.024	0.012	0.054	0.013	0.032	0.019	0.045	0.032	0.055	0.036	0.050
Sub9	***Mean***	0.842	0.179	0.824	0.138	0.832	0.190	0.820	0.161	0.828	0.166	0.104
	SD	0.025	0.022	0.032	0.003	0.031	0.021	0.040	0.016	0.037	0.027	0.023
Sub10	***Mean***	0.817	0.158	0.775	0.116	0.875	0.186	0.830	0.185	0.825	0.162	0.197
	SD	0.033	0.023	0.023	0.005	0.025	0.027	0.027	0.036	0.062	0.042	0.030
Mean	***Mean***	0.826	0.154	0.746	0.120	0.841	0.185	0.756	0.165	0.789	0.156	0.146
	SD	0.027	0.018	0.073	0.011	0.034	0.022	0.063	0.027	0.084	0.038	0.025

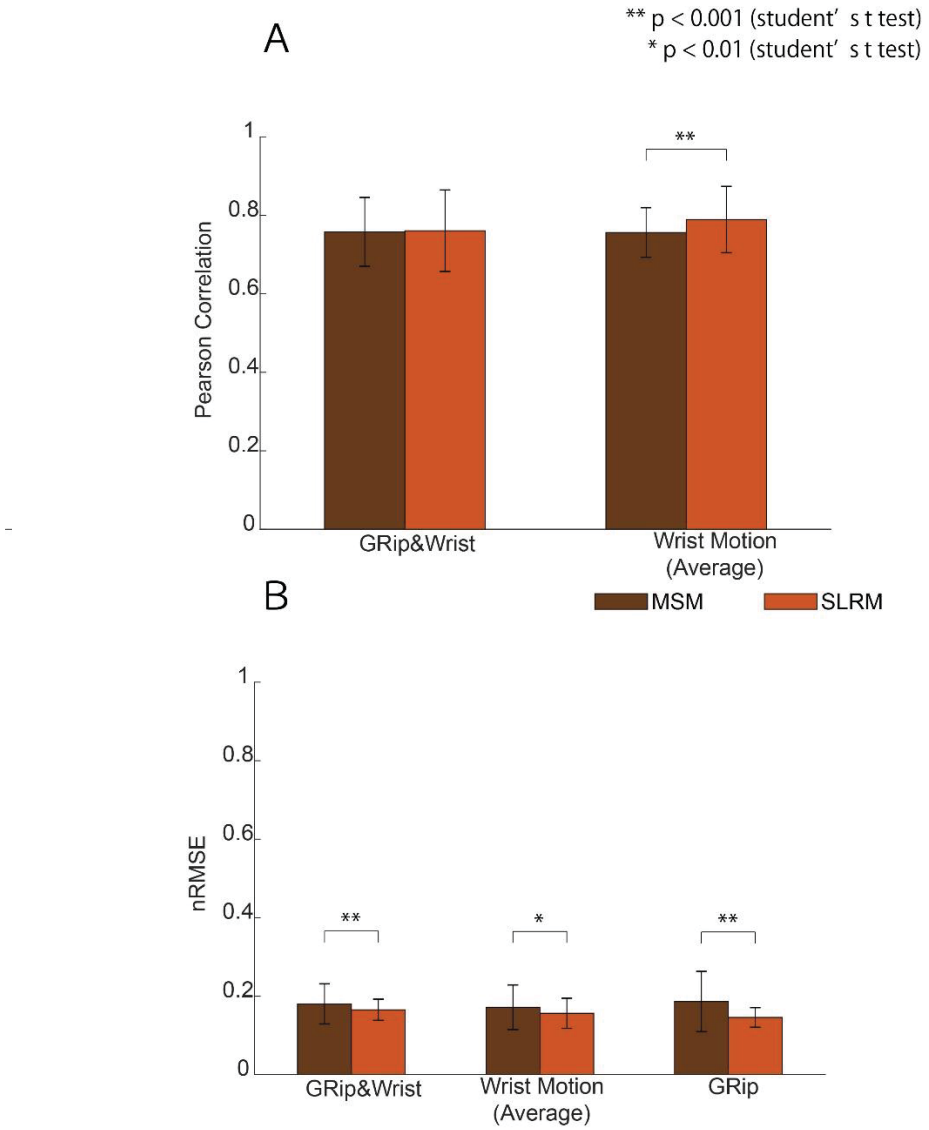

Figure 3.7 Trial based wrist joint movement estimation performance changes in synergy-based linear regression model (SLRM) and musculoskeletal model (MSM) in terms of Pearson correlation coefficient (r) and normalized root mean square error (nRMSE). (A) SLRM and MSM had no statistically significant difference in wrist motion with grip, while wrist motion average had a statistically significant difference between the models ($p < 0.001$, Student's t-test). (B) nRMSE between SLRM and MSM had a statistically significant difference in every trial.

C. Task2 - Grip Motion Test

Figure 3.8 shows the continuous grip force estimates under SLRM and the following angle estimate perturbation. I asked participants to fasten their hand on a grip device what restricted wrist motion during the task. Hence, I monitored the grip task not only the grip force estimation but also wrist angle estimation. There checked whether grip motion muscle activity affects the angle estimate under SLRM. The results showed that during the gripping task, instability of the wrist angle estimation occurred in the presence of a strong force activation, as may be seen in Figure 3.8 (D). For the half and quarter grip force task, angle estimation was less than 30 degrees, as shown in Figure 3.8 (E) and (F). The r value for grip force estimation and nRMSE of the X-Y angle estimation, compared with zero angle (no movement), were computed as indicated in Table 3-4. Sub 8 data was omitted in this task because the EMG signal was saturated during the analog to digital converting process using National Instrument Data Acquisition (±5 voltage). The SLRM-based grip-force estimate from nine participants was 0.846 ± 0.050 in r with 0.256 ± 0.140 nRMSE in wrist movement estimation.

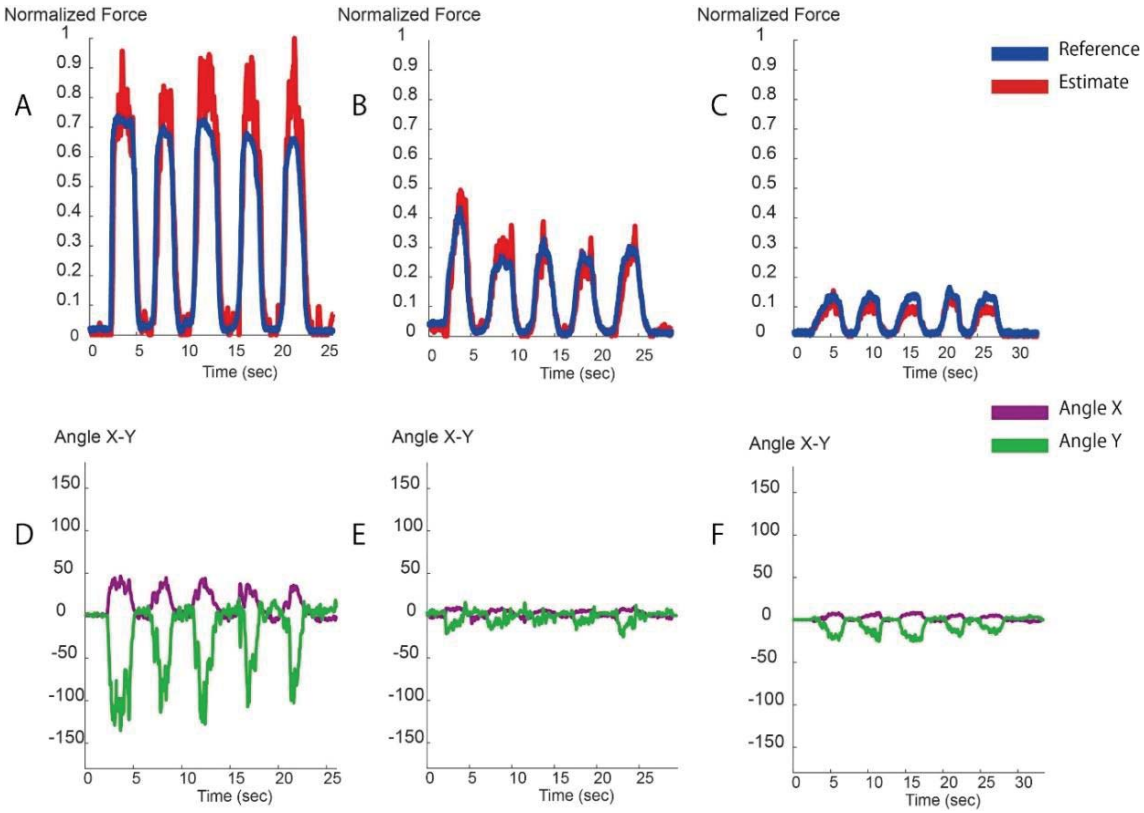

Figure 3.8 Times series estimation of grip task with ReachMAN robot. (A) Time series for the normalized max grip force reference and synergy-based linear regression (SLRM) grip force estimate. (B) Time series for the normalized half grip force reference and synergy-based linear regression (SLRM) grip force estimate. (C) Time series for the normalized quarter grip force reference and synergy-based linear regression (SLRM) grip force estimate. (D) Time series for wrist joint motion estimate from SLRM in max grip force task. (E) Time series for wrist joint motion estimate from SLRM in half grip force task. (F) Time series for wrist joint motion estimate from SLRM in quarter grip force task. Angle X -Y is the same axis in Figure 3.6

Table 3-4. SLRM grip force estimates per participant with corresponding wrist movement estimate perturbation

Sub		Grip Force Estimate (*r*)		Angle X-Y error (nRMSE)	
		(Average)	(std)	(Average)	(std)
Sub1	Mean / SD	0.844	0.021	0.307	0.075
Sub2	Mean / SD	0.716	0.058	0.453	0.192
Sub3	Mean / SD	0.791	0.124	0.093	0.076
Sub4	Mean / SD	0.893	0.018	0.198	0.037
Sub5	Mean / SD	0.868	0.042	0.316	0.119
Sub6	Mean / SD	0.953	0.010	0.275	0.165
Sub7	Mean / SD	0.949	0.013	0.200	0.173
Sub8	Mean / SD				
Sub9	Mean / SD	0.859	0.032	0.244	0.026
Sub10	Mean / SD	0.747	0.020	0.218	0.232
Mean	Mean / SD	0.846	0.050	0.256	0.140

3.8 Discussion

This chapter tested continuous hand motion estimation using SLRM with a comparison of MSM. As explained by Kawase et al (2017), MSM also had a robustness of the wrist movements in relation to finger movement. However, the SLRM wrist movement estimation outperformed with statistical significance in nRMSE under any trials and even *r* except the complex movement of grip & wrist trial. The goal of this study is to use outcome models in practical such as prosthesis or the interface. For this reason, only basic noise attenuation which is mainly applied at the sensor level was applied in the

EMG. Therefore, even with the anatomical placements of the EMG signal, some noise remains depending on the subject with low signal-to-noise-ratio. Unlike MSM, which is based on signals in each channel, SLRM appears to show higher robustness in this environment because it utilizes EMG coactivation.

The estimation performance of SLRM showed comparable performance with previous results in the literature on trajectory (Castellini & Van, 2009) and joint force (Jiang, et al., 2012) estimation in spite of small amount of training data. The advantage of SLRM is not only continuous wrist movements but also complex movements. The wrist movement estimation performance was equivalent and better at some point compared to MSM performance.

Within the wrist-only motion trials, both SLRM and MSM had the lowest performance in comfortable half performances. It is most likely due to the non-linearity between EMG signals and arm motion, or contamination of movement artifact and baseline noise to the EMG (representatively, Sub3). Therefore, the non-linear regression techniques used in previous studies (Castellini & van der Smagt, 2009; Jiang et al., 2012) could be comparable with the synergy-based model having an alternative to using linear regression.

The linear envelope filtering used in the EMG signal analysis was proven to have highly correlated signals with joint torque induced by the target muscle (Koike & Kawato, 1995). Grip synergy, which is a co-activation of these filtered EMG signals, also showed a high grip force estimation performance having correlation of 0. 846 ± 0.050 without resort to further conversion or regression techniques in nine participants. The gripping force level did not affect the estimation performance. In movement intention

discrimination performance, however, the strong grip-trial showed wrist angle estimation distortion. This strong-grip distortion indicates the necessity to investigate the limits of the SLRM in grip force estimation. The current result alone cannot determine which parameter triggers the distortion of wrist angle estimation. It could be a specific physical force or a particular ratio of the maximum force level, or other causality.

3.9 Conclusion

This chapter conducted continuous wrist joint angle estimation with/without gripping. In the first task, I compared SRLM and MSM for the wrist angle estimation performance. The SLRM exhibited relatively higher performance in wrist motion. In the gripping, SLRM showed robustness in angle estimation when the grip force is half or a quarter of its maximum force level. Also, SLRM could provide the extent of grip force exerted in the center-position with little perturbation. These characteristics of SLRM can be useful for combined wrist and grip motion estimation. Thereby, this result showed the feasibility of superficial muscle activity separation; however, there should be a limitation on the grip force not to crash the wrist angle estimation and vice versa. Further studies are required to obtain and test the simultaneous regression of both angle and grip force necessary for real-life applications. Based on the current result of superficial muscle activity identification, the next step began looking for deep muscle activity identification and their resultant posture recognition.

Chapter 4 Finger Movement Estimation from High Density EMG

4.1 Introduction

This chapter tested the separation of the superficial and deep muscle signals in high-density EMG data. As mention in the background, surface EMG signals contain different muscle signals and various noises such as baseline noise and movement artifacts (De Luca, et al., 2010). These noises and crosstalk between muscles can misguide EMG analysis leading to erroneous interpretation; hence, various studies focus on attenuating undesirable signals (De Luca, et al., 2010). However, it is still challenging to detect single muscle activity from EMG sensors (Keen & Fuglevand, 2004; Schieber, 1995). Gazzoni et al., (2014) applied NMF to high-density EMG signals. Then they distinguished the muscle position on each forearm per movement of the wrist and single finger joint. Their deep muscle position investigation showed the feasibility of high-density EMG analysis in deep muscle identification. However, they could not step further toward natural movement nor the structure of muscle synergy per joint movement. Finger movements of high dexterity generate multiple muscle activations; however, this causes significant crosstalk in the forearm EMG measurements. Thereby, additional steps need to be taken in dexterous finger movement estimation using a high-density EMG signal.

Independent component analysis (ICA) is a general-purpose statistical technique that can linearly transform random data into independent components (ICs) (Hyvärinen & Oja, 2000). Hence, it is one of the most important algorithms in biomedical signal processing, especially for EEG, where noise and various movement artifacts reduction is critical. In EEG, such noises are removed through ICA before signal analysis (Jung, et al., 2000). Even in EMG analysis, Staudenmann et al. (2007) revealed that ICA reduces the

root mean squared error of the monopolar EMG signals when measuring muscle force. The NMF algorithm by Lee and Seung (2001) has established a standard method for muscle synergy calculation. Since then, several EMG studies have proposed low-dimensional input-based myoelectric models using muscle synergy. However, NMF in high-density EMG analysis caused problems by the normalization process. Normalization modulates each channel size equal to have 1 in maximum. But most high-density EMGs contain merely noise components. Therefore, there demands several techniques and know-how to resolve this problem beforehand. Since NMF alone cannot distinguish significant signals among EMG sensor signals, ICA applied in the raw EMG signals.

This chapter tests how well high-density EMG signals can estimate the direction of index finger movements. There applied two signal decomposition ICA and NMF. In the previous chapter, NMF showed feasibility in estimating complex wrist and grip motion. Thereby, three parameters following were examined to compare NMF alone (EMG-synergy) and sequential ICA and NMF analysis (IC-synergy). 1. robustness of the synergy structure calculation in the two elbows posture, 2. The robustness of preferred direction compared per elbow posture, and 3. classification performance on the eight direction finger movements using convolutional neural network (CNN).

4.2 Experimental Procedure

This study used experimental data obtained from Yoshimura et al. (2017). Six healthy right-handed participants (two females and four males, aged 40.7±7.2) joined the experiment. The research protocol was approved by the University of California San Diego Ethics Committee (approval number 14353) and was conducted following the Helsinki Declaration. Written consent was obtained from each participant before the experiment (Yoshimura, et al., 2017). This study focused on 96 channel EMG signals

acquired from the Biosemi active Two amplifier system with active sensors (Biosemi, Amsterdam, Netherlands), and its analysis concerning cursor movement directions. The EMG signals were sampled at 2048 Hz and Cursor movement at 100 Hz.

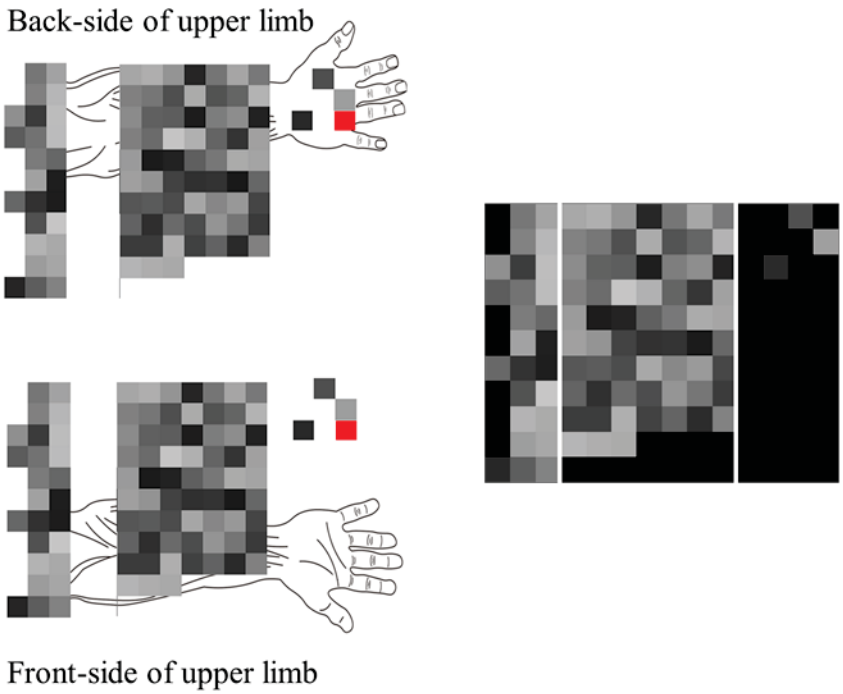

Figure 4.1. EMG signals with respective channel positions on the upper limb. The red channel on the back of the hand is used as the ground and not for ICA or muscle synergy.

The posture functional capacity evaluation system (zebris Medical GmbH, Isny, Germany) measured EMG sensors and joint positions on the arm. The abstract EMG sensor placements are as in Figure 4.1.

The participants performed finger movements shifting the cursor in eight different directions at two elbow angles (0° and 90°) shown in Figure 4.1. The numbering of directions per posture was constant to extract the extrinsic coordinate reaction. They repeated movements 80-times per each posture and action.

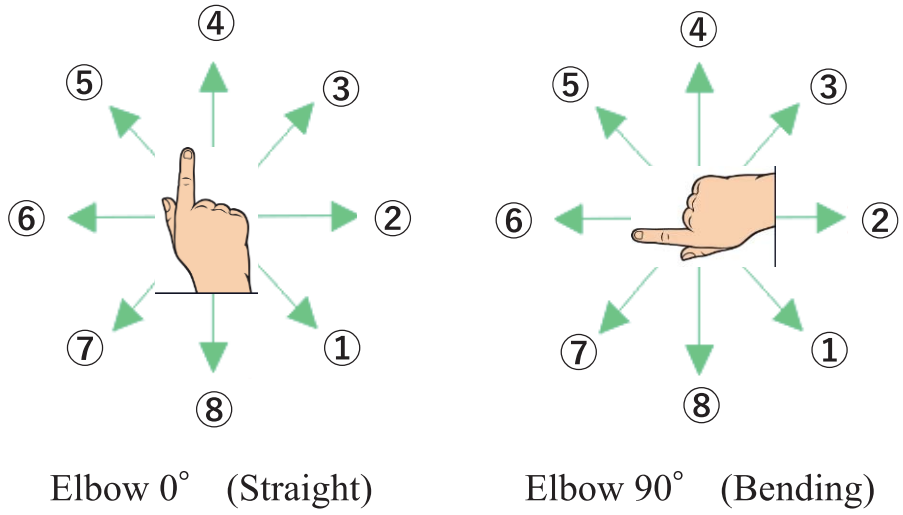

Figure 4.2. Eight target directions for the two different elbow angles (0° and 90°)

In the experiment, each participant placed their right forearm on an arm rest (350-series, Ergorest, Siilinjarvi, Finland) and wrist on a desk., The task was moving the cursor on the monitor using the right index finger on a touchpad (T650, Logitech, Lausanne, Switzerland) in one of two elbow angles refraining arm movement. Each trial ran 4 s composed of 2s of preparation and 2 s of movement. In the prior, a red circle cursor appeared on the center of monitor with participants placing their index fingers at the center of the touchpad. In the latter, a target circle appeared randomly at one of eight positions distributed 45° apart on a circle with a 10-cm radius for the next 2 s. The participants got the instruction to move at once per trial. It was even when the final cursor position is displaced far from the target. When the target disappeared, participants moved their index fingers back to the center origin so as to conduct the next trial. The participants completed 80-time repetitions on each posture and direction described in Figure 4.2.

4.3 Data Acquisition and Preprocessing

Data analysis was upon the Matlab program. The experimental data went down the Matlab. EMG gets digitally filtered by the 50 Hz notch and 10-1000 Hz band-pass filters. Then, there computed standard deviation on each EMG sensor, and the least vibrating sensor became the ground reference. The sensor in six participants was in the same position, on the back of the hand. Having one channel and as a ground reference, in ICA computation, the number of EMG sensors becomes ninety-five. ICA is one of the famous BSS methods and frequently used cases like the cocktail party problem. High-density EMG signals scattered on the forearm without any anatomical basis. Thereby in some channel data, the signal-to-noise ratio was too low that muscle activities and noises are indistinguishable. For this reason, ICA analysis was carried out after the preprocessing to derive deep muscle activities. In a matrix formula, ICA is deriving

$$X = AS \tag{7}$$

where X is C by N EMG signal matrix, C is the number of input channels and N is time points. S is C by N IC matrix where the vectors are expected mutually independent, and A is C by C square matrix showing how the source signal S is composed in each sensor. ICA derives the basis vectors in the way minimizing the mutual information and maximizing the non-Gaussianity. Each trial had a 2 s duration, the post-onset recording after target onset. Among the outputs from AMICA, I excluded ICs that show white noise characteristics upon trials-based average. The selective ICA analyzed from the 95 channel EMG signals on 1280 trials out of the six participants yielded between 22 to 36 ICs varying per participant (mean: 29.8, standard deviation (SD): 5.1).

In the synergy computation, IC-synergy chose three to fifteen sets, and EMG-synergy three to thirty per participant. When selecting the synergy number, the following two conditions became the standard each different per participant: more than 0.9 Variance Account For (VAF) that commonly applied in other studies (Cheung et al., 2005; Clark et al., 2010; Santuz et al., 2017) and less than 10^{-4} mean squared error of the linear regression of VAF per muscle synergy number (d'Avella, et al., 2006). Figure 4.4 shows two condition parameters with the number of IC-synergy in six participants. From these conditions, 10 to 26 EMG-synergy (mean: 18.2, SD: 5.5) and 9 to 18 IC-synergy (mean: 12.2, SD: 3.2) were derived from the whole dataset and used depending on the participants throughout the study.

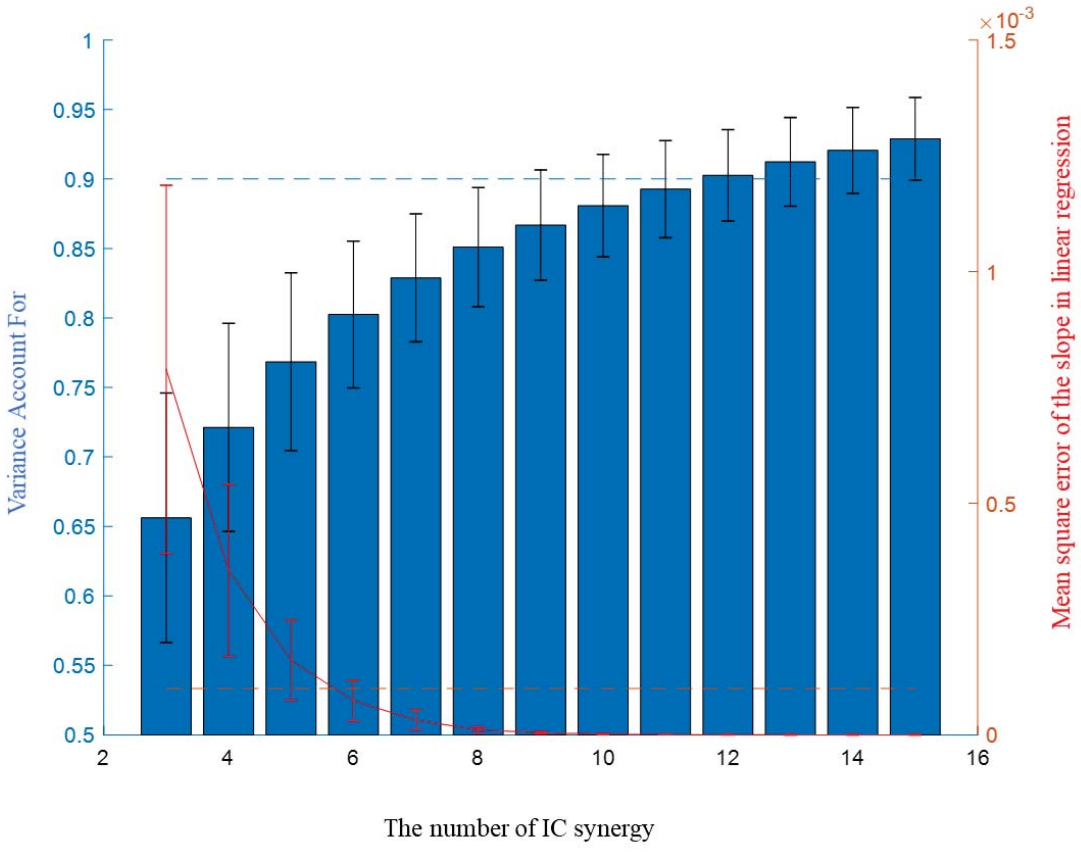

Figure 4.3. Mean Variance Account For (VAF) and slope of VAF of IC synergy in the six participants

In addition to the entire dataset-based synergy computation, I derived muscle synergies from each postural dataset (Elbow 0°, Elbow 90°). In this computation, there applied the same number of synergies to see the consistency of the structure.

I clustered the synergies from three different datasets and then grouped the muscle synergies depending on the scalar product (Cheung et al., 2012; Matsunaga et al., 2017) using the Unweighted Pair-Group Method with Arithmetic mean (Nei & Kumar, 2000). The module criteria were the scalar product of more than 0.75. Cosine tuning calculated the preferred direction of the muscles and synergies using the average amplitude of eight direction movement trials. The detail is muscle (or synergy) signal m(θ) in eight direction θ with a linear regression $m(\theta) = a_0 + a_1 \cos(\theta) + a_2 \sin(\theta)$ (Gentner, et al., 2013). The preferred direction of the signal (either muscle or synergy) is $\theta^{PD} = \tan^{-1}(a_2/a_1)$. Then the resultant preferred directions are compared within a module to verify the signal consistency in two elbow postures. The preferred directions of the synergy in Elbow 90 were compensated by shifting 90° clockwise. In cosine tuning linear regression under the normalized form, cosine tuning weight is defined as $W = \sqrt{a_1^2 + a_2^2}$, which shows the muscle activation ratio for target finger movements.

4.4 Classification Model

Before the classification, all input signal was down-sampled to 50hz to reduce the computational cost. In addition, the data cut off from -0.2 second to 0.3 seconds on the basis of the movement initiation. However, it is difficult to grasp a precise onset using EMG due to noise, so there used cursor movements as the cut off reference. When the cursor had more than 2% of the final distance became the onset timing. There used four different types of muscle activity signals: EMG-input, IC-input, EMG-synergy, and IC-

synergy for classification. Twenty-five-time points of high-density signal set were given as input signal for CNN (Krizhevsky, et al., 2012) to classify the eight directional finger movements. In CNN, the three by three 32 filters extracted features and five-fold cross-validation conducted on the whole datasets dividing each elbow posture individually.

4.5 Results

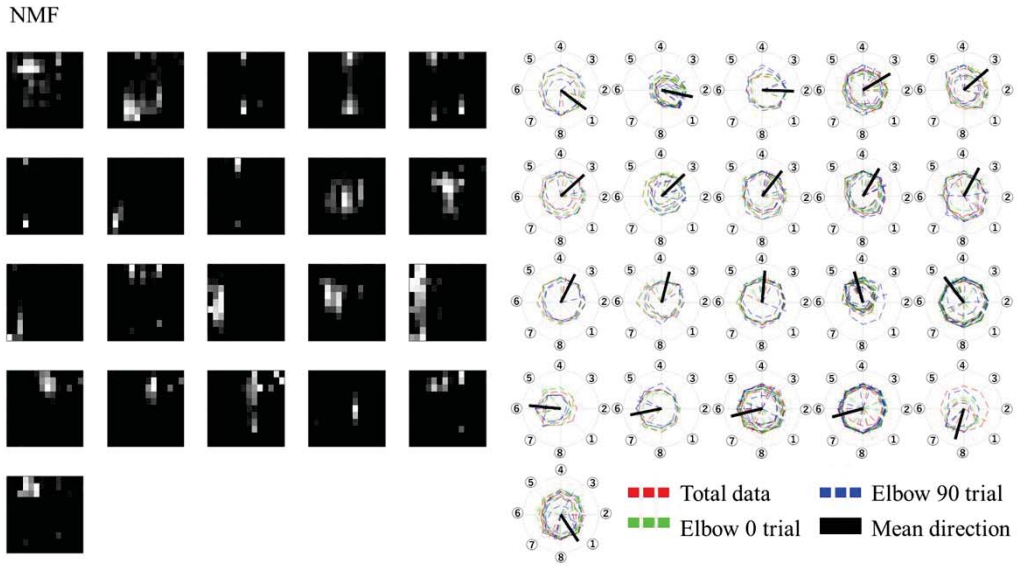

Figure 4.4. NMF Synergy Modules with corresponding preferred directions. The preferred direction was expressed in different colors according to the trial. Red represents total data, Green represents Elbow 0 trial, Blue represents Elbow 90 trial.

When grouping synergies into modules from different elbow posture conditions, the number of EMG-synergy modules was proportional to the EMG-synergy number (e.g., i.e., the ratio between module and synergy is 14.4 modules out of:18.2 synergies in six participants). On the contrary, the module number of IC-synergy was between eight and ten that is independent to the IC-synergy number (nine to eighteen). Figure 4.4 and Figure 4.5 show the EMG channel activations of EMG-synergy and IC-synergy modules from an individual participant.

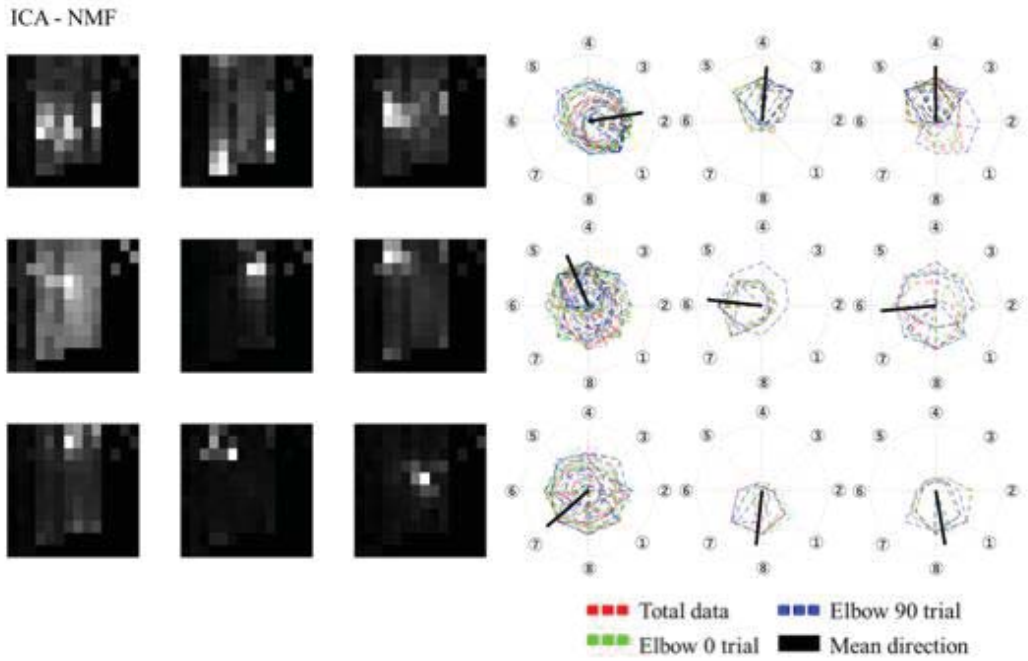

Figure 4.5. ICA-NMF Synergy Modules with corresponding preferred directions. The preferred direction was expressed in different colors according to the trial. Red represents total data, Green represents Elbow 0 trial, Blue represents Elbow 90 trial.

Between EMG-synergy (Figure 4.4) and IC-synergy (Figure 4.5) modules, some modules had similar EMG channel activation with more than 0.75 scalar product. But their inclination for each finger movement is significantly different. The average cosine tuning weight W is bigger in IC-synergy than that of EMG-synergy module ($p < 0.0001$, $W_{ICA} = 0.34 \pm 0.11$, $W_{EMG} = 0.18 \pm 0.12$, $n = 35$). As in Figure 4.4 and W, EMG-synergy showed similar muscle activation channels with IC-synergy, but the movement-related signal ratio was almost half of IC-synergy. It affects the wrong preferred direction computation so that the average preferred-direction-error within the EMG-synergy module is 24.4±25.8°. As in Figure 4.5, IC-synergy modules are likely to indicate one clear direction so that the average preferred-direction-error within the modules is 13.4±18.1°. The preferred direction robustness per elbow posture differed statistically significantly between the two cases for the t-test ($p = 0.0069$, $n_{EMG} = 87$, $n_{ICA} = 54$).

The shape of the structure categorized EMG-synergy and IC-synergy modules into two different types, i.e., (i) parallel type wherein the EMG activations shaped alongside the forearm, and (ii) local type wherein the EMG activations are structured in the cross-sectional region of the forearm. Figure 4.6 shows the synergy module changes of parallel and local type per input with corresponding EMG channel activations. For the parallel type, both input-based synergies showed similar EMG channel coactivation and preferred direction. It pointed toward a specific finger movement, which is the flexion of the index finger. However, in the local type, EMG-synergy did not have the preferred direction. And the preferred direction of the corresponding EMG channels is also very vague. But when looking at the IC-synergy in this type, it showed similarity to those of parallel one.

In finger movement direction estimation, there applied CNN classification per each input (EMG-input, IC-input, EMG-synergy, and IC-synergy) per coordinate (i.e., extrinsic and intrinsic coordinates). Naturally, intrinsic coordinate always showed a higher classification performance than the extrinsic for all inputs. (Extrinsic vs. Intrinsic: $p_{EMG\text{-}input} < 0.0001$, $p_{IC\text{-}input} = 0.0013$, $p_{EMG\text{-}synergy} = 0.0034$, $p_{IC\text{-}synergy} = 0.011$, $n = 30$). Therefore, I compared all the classification performance on the intrinsic coordinate. And the classification performances per input are shown in Figure 4.6 to 4.10 as confusion matrices. The results show that there is no statistical difference before and after synergy computation both in EMG and ICA. (EMG-input vs. EMG-synergy, $p = 0.18$, IC-input vs. IC-synergy, $p = 0.86$, $n = 30$). And the presence or absence of ICA drastically changed the performance (EMG-input vs. IC-input, $p < 0.0001$, EMG-synergy vs. IC-synergy, $p < 0.0001$, $n = 30$).

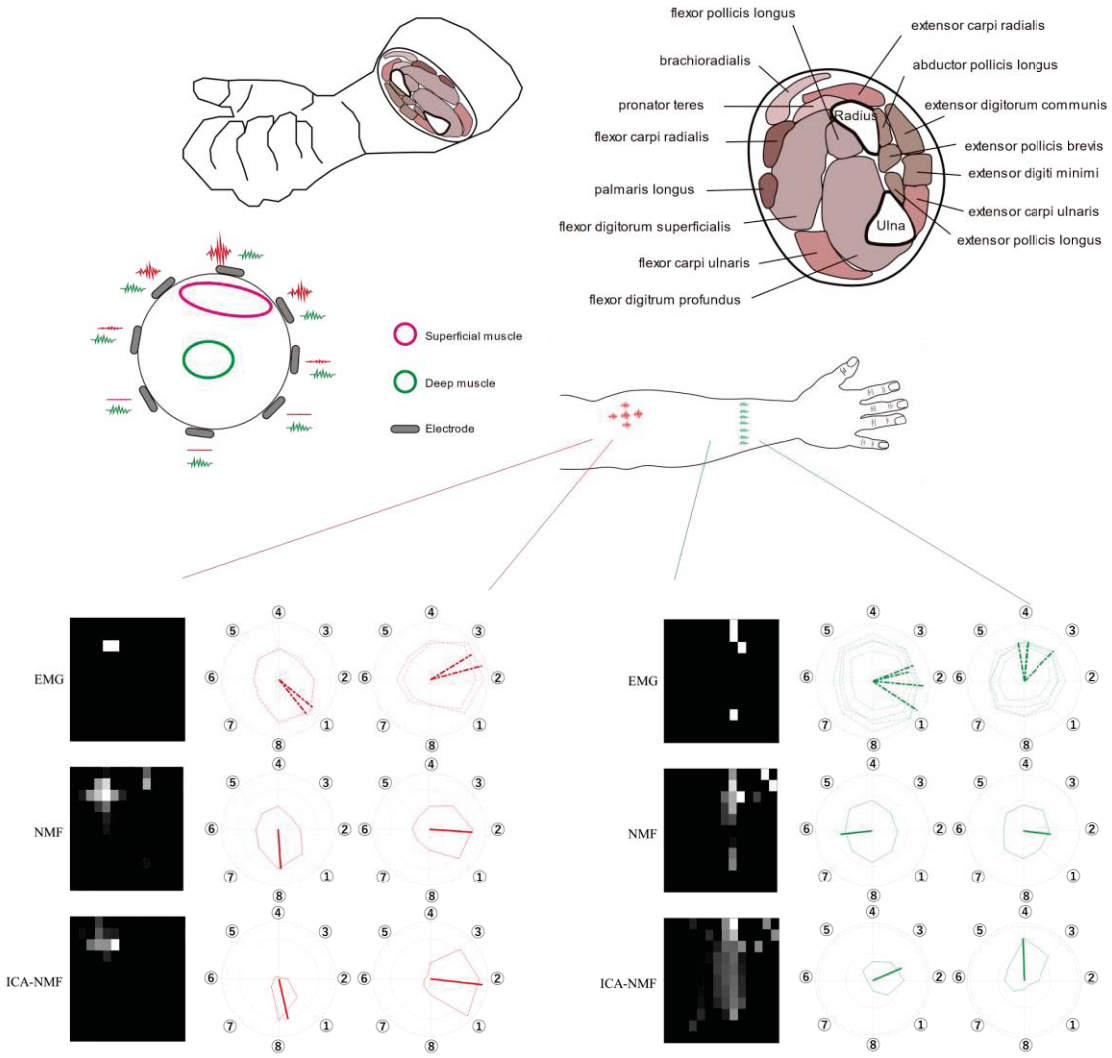

Figure 4.6. Comparison of horizontal (alongside of the forearm) and vertical (cross-sectional side of the forearm) structure synergy in participants. Considering the physical placement of the muscles, horizontal synergy was expected to be a superficial muscle activity and vertical one as a deep muscle activity. The horizontal structure synergy (Red) had equivalent preferred direction both in NMF and ICA-NMF computation while vertical structure synergy (Green) had distinctive preferred direction change between NMF and ICA-NMF synergy.

Intrinsic - EMG

	①	②	③	④	⑤	⑥	⑦	⑧
①	522 (59.18%)	158 (17.52%)	30 (3.47%)	26 (2.80%)	12 (1.35%)	11 (1.21%)	13 (1.50%)	107 (11.93%)
②	179 (20.29%)	487 (53.99%)	177 (20.49%)	74 (7.96%)	34 (3.84%)	34 (3.74%)	29 (3.35%)	53 (5.91%)
③	19 (2.15%)	127 (14.08%)	431 (49.88%)	198 (21.29%)	20 (2.26%)	9 (0.99%)	7 (0.81%)	11 (1.23%)
④	8 (0.91%)	39 (4.32%)	166 (19.21%)	531 (57.10%)	87 (9.82%)	7 (0.77%)	6 (0.69%)	19 (2.12%)
⑤	19 (2.15%)	28 (3.10%)	28 (3.24%)	58 (6.24%)	471 (53.16%)	193 (21.21%)	61 (7.04%)	27 (3.01%)
⑥	11 (1.25%)	15 (1.66%)	10 (1.16%)	11 (1.18%)	186 (20.99%)	447 (49.12%)	201 (23.21%)	35 (3.90%)
⑦	7 (0.79%)	4 (0.44%)	5 (0.58%)	6 (0.65%)	44 (4.97%)	169 (18.57%)	470 (54.27%)	98 (10.93%)
⑧	117 (13.27%)	44 (4.88%)	17 (1.97%)	26 (2.80%)	32 (3.61%)	40 (4.40%)	79 (9.12%)	547 (60.98%)

Figure 4.7. Confusion Matrix of four different input types on Intrinsic Coordinate with EMG 95ch inputs

Intrinsic - NMF

	①	②	③	④	⑤	⑥	⑦	⑧
①	577 (65.42%)	133 (14.75%)	8 (0.93%)	13 (1.40%)	18 (2.03%)	11 (1.21%)	5 (0.58%)	106 (11.82%)
②	163 (18.48%)	553 (61.31%)	195 (22.57%)	63 (6.77%)	16 (1.81%)	9 (0.99%)	1 (0.12%)	7 (0.78%)
③	8 (0.91%)	115 (12.75%)	435 (50.35%)	180 (19.35%)	21 (2.37%)	3 (0.33%)	0 (0.00%)	7 (0.78%)
④	3 (0.34%)	44 (4.88%)	186 (21.53%)	584 (62.80%)	74 (8.35%)	12 (1.32%)	3 (0.35%)	16 (1.78%)
⑤	11 (1.25%)	16 (1.77%)	26 (3.01%)	74 (7.96%)	504 (56.88%)	202 (22.20%)	57 (6.58%)	17 (1.90%)
⑥	6 (0.68%)	3 (0.33%)	4 (0.46%)	7 (0.75%)	181 (20.43%)	432 (47.47%)	208 (24.02%)	22 (2.45%)
⑦	3 (0.34%)	5 (0.55%)	3 (0.35%)	0 (0.00%)	52 (5.87%)	212 (23.30%)	517 (59.70%)	85 (9.48%)
⑧	111 (12.59%)	33 (3.66%)	7 (0.81%)	9 (0.97%)	20 (2.26%)	29 (3.19%)	75 (8.66%)	637 (71.01%)

Figure 4.8. Confusion Matrix of four different input types on Intrinsic Coordinate with NMF synergies

(mean: 18.2, SD: 5.5)

Intrinsic - ICA

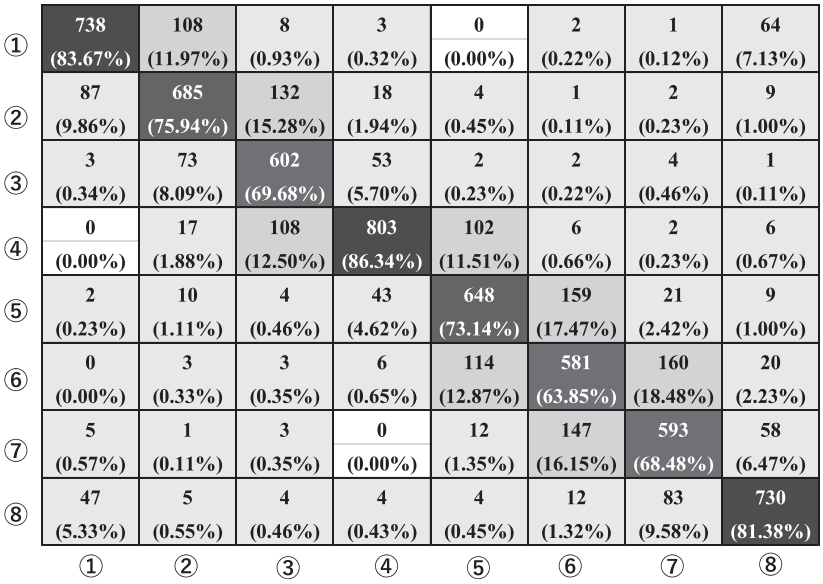

	①	②	③	④	⑤	⑥	⑦	⑧
①	738 (83.67%)	108 (11.97%)	8 (0.93%)	3 (0.32%)	0 (0.00%)	2 (0.22%)	1 (0.12%)	64 (7.13%)
②	87 (9.86%)	685 (75.94%)	132 (15.28%)	18 (1.94%)	4 (0.45%)	1 (0.11%)	2 (0.23%)	9 (1.00%)
③	3 (0.34%)	73 (8.09%)	602 (69.68%)	53 (5.70%)	2 (0.23%)	2 (0.22%)	4 (0.46%)	1 (0.11%)
④	0 (0.00%)	17 (1.88%)	108 (12.50%)	803 (86.34%)	102 (11.51%)	6 (0.66%)	2 (0.23%)	6 (0.67%)
⑤	2 (0.23%)	10 (1.11%)	4 (0.46%)	43 (4.62%)	648 (73.14%)	159 (17.47%)	21 (2.42%)	9 (1.00%)
⑥	0 (0.00%)	3 (0.33%)	3 (0.35%)	6 (0.65%)	114 (12.87%)	581 (63.85%)	160 (18.48%)	20 (2.23%)
⑦	5 (0.57%)	1 (0.11%)	3 (0.35%)	0 (0.00%)	12 (1.35%)	147 (16.15%)	593 (68.48%)	58 (6.47%)
⑧	47 (5.33%)	5 (0.55%)	4 (0.46%)	4 (0.43%)	4 (0.45%)	12 (1.32%)	83 (9.58%)	730 (81.38%)

Figure 4.9. Confusion Matrix of four different input types on Intrinsic Coordinate with Independent Components (mean: 29.8, standard deviation (SD): 5.1)

Intrinsic – ICA-NMF

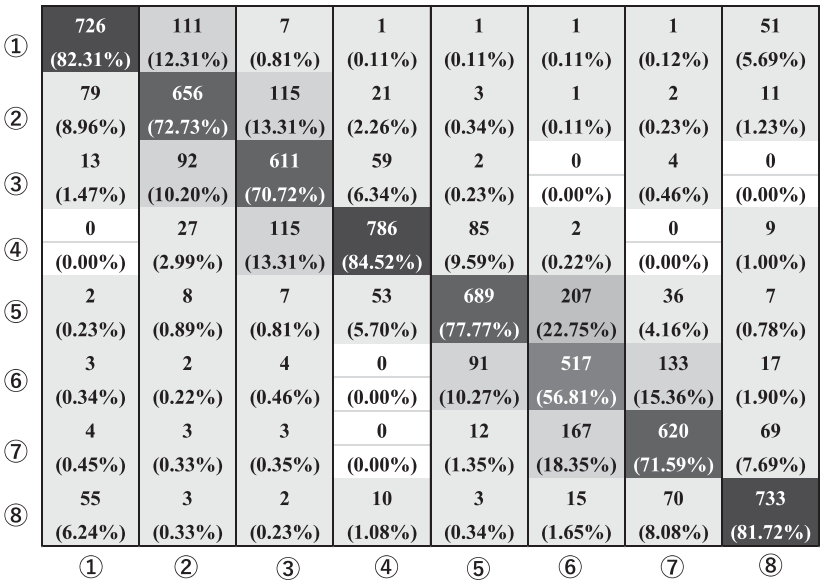

	①	②	③	④	⑤	⑥	⑦	⑧
①	726 (82.31%)	111 (12.31%)	7 (0.81%)	1 (0.11%)	1 (0.11%)	1 (0.11%)	1 (0.12%)	51 (5.69%)
②	79 (8.96%)	656 (72.73%)	115 (13.31%)	21 (2.26%)	3 (0.34%)	1 (0.11%)	2 (0.23%)	11 (1.23%)
③	13 (1.47%)	92 (10.20%)	611 (70.72%)	59 (6.34%)	2 (0.23%)	0 (0.00%)	4 (0.46%)	0 (0.00%)
④	0 (0.00%)	27 (2.99%)	115 (13.31%)	786 (84.52%)	85 (9.59%)	2 (0.22%)	0 (0.00%)	9 (1.00%)
⑤	2 (0.23%)	8 (0.89%)	7 (0.81%)	53 (5.70%)	689 (77.77%)	207 (22.75%)	36 (4.16%)	7 (0.78%)
⑥	3 (0.34%)	2 (0.22%)	4 (0.46%)	0 (0.00%)	91 (10.27%)	517 (56.81%)	133 (15.36%)	17 (1.90%)
⑦	4 (0.45%)	3 (0.33%)	3 (0.35%)	0 (0.00%)	12 (1.35%)	167 (18.35%)	620 (71.59%)	69 (7.69%)
⑧	55 (6.24%)	3 (0.33%)	2 (0.23%)	10 (1.08%)	3 (0.34%)	15 (1.65%)	70 (8.08%)	733 (81.72%)

Figure 4.10. Confusion Matrix of four different input types on Intrinsic Coordinate with ICA-NMF synergies (mean: 12.2, SD: 3.2)

4.6 Discussion

The goal of this multi-EMG analysis is to elucidate the effect of ICA and NMF in reducing crosstalk. EMG signals are derived from overlaid muscles both superficial and in depth. EMG signals originate from overlaid muscles superficial and in-depth with noise components. By investigating the preferred direction and movement direction decoding, I checked the accuracy and precision increase with and without ICA and NMF. The synergy modules from three different data (Elbow 0 and 90, and whole dataset) showed that most NMF results in finger movement EMG signal were consistent in elbow postures. But when considering the classification performance using CNN, such compatible synergy modules did not give accurate finger movement estimation. On the other hand, In ICA-NMF, the number of modules (8 to 10) was close to the number of finger movements (8) with other synergies being relevant to elbow posture. meanwhile, the classification performance using CNN was the highest in IC-synergy input. This outcome matches the result of Staudemann et al., (2007) showing that ICs improved muscle force estimation. Eight to ten IC-synergy modules were the coactivations for finger movements, and others might be unrelated muscle movements that need to be investigated further.

The modularization of muscle synergies and the shifted preferred direction confirmed that they belong to intrinsic coordinates. Even the classification performances were higher than the extrinsic coordinate at all times. Therefore, the target of EMG decoders should be intrinsic parameter when developing EMG based interfaces or applications. The muscles synergy module had structures in two big categories with a small number of outliers. The index finger-based cursor movements in 8 directions require participants to activate superficial and deep muscles placed in a multi-layer

structure on the forearm (Blanc & Dimanico, 2010). Because of the physical location, the signal distribution on multiple EMG sensors would vary depending on where the muscle derives from. It is assumed that the superficial would appear in parallel modules while the deep would appear in the cross-sectional modules. The inner muscle activity dissipates in omnidirectional so that it forms evenly and widely in the cross-sectional region of the forearm.

Even though EMG passed preprocessing, there could still exist the crosstalk and other heterogeneous noises. They make muscle reaction blurry, and it is more likely to happen in deep muscle signals because they should have less signal to noise ratio than the superficial. Upon this condition, ICA takes the role of sensor configuration (Staudenmann, et al., 2006) or replacement of temporal whitening (Clancy & Hogan, 1995). It separates noise and EMG artifacts, even sorting out muscle activities, maximizing independent component dimensionality to input signal dimension. NMF after ICA reassembled the muscle coactivation in a predefined number of synergies. This way, IC-synergy succeeded in classifying the superficial and deep muscles that led to robust finger movement classification with a few inputs. Thus, finger movement estimation represents the necessity of ICA on the high-density EMG before muscle synergy derivation, which even holds the minimum number of input channels. The ICA and NMF role become clear in in CNN classification performance. The ICA and NMF roles become clear in CNN classification performance. ICA increased classification performance accuracy while NMF minimized the input dimensions, saving computational cost. The 95 EMG channels downsize to 18.2 ± 5.5 EMG synergies, 29.8 ± 5.1 ICs to 12.2 ± 3.2 IC synergies.

4.7 Conclusion

This study investigated the effect of ICA and NMF in high-density EMG signals. EMG had an intrinsic coordinate, and its derivative parameters after ICA and NMF maintained the characteristic. The high-density EMG analysis confirmed that the ICA increased the classification accuracy by detecting deep muscle activation. NMF did not affect the classification performance but reduced the input dimension. NMF could not attenuate the noise component from the deep muscle activity. Meanwhile, ICA-NMF showed a clear preferred direction in both superficial and deep muscles. Of course, it is still necessary to check whether the IC synergy could divide mixture of superficial and deep muscle signals under more complex movement including multiple finger and wrist movement coactivation. In addition, the current estimations only progressed up to the classification stage. The studies on the wrist or upper joint movements mainly focused on the trajectory (Xia, et al., 2018) and the joint angle estimation (Kawase, et al., 2017) at a continuous level what prosthesis user required (Biddiss, 2009). Thereby, further research is still demanding to connect and check the feasibility of this current IC synergy input to continuous estimation models.

Chapter 5 Consideration in Muscle Synergy Computation

5.1 Synergy Derivation per Individual DOF Trial

When deriving muscle synergy, synergy matrices depend highly on task constraints (Roh, et al., 2012). One solution is to calculate the muscle synergy per each fundamental movement (Furui, et al., 2019). However, this not only increases the training session but also make synergies to be vulnerable to unexpected noises at the trials. As a way to compromise, chapter 3 computed the muscle synergy per wrist and grip trial. Figure 5.1 describe the necessity of movement-type separation in synergy derivation (wrist movements and gripping). The synergy set from the joint trials is SLRM1, and that of the separate trials is SLRM2. The time series synergy coefficients in Figure 5.1 are derived from the pre-defined two different models at the gripping task. SLRM1 divides the seven-channel EMG signals into several part-based synergy groups without movement type consideration, resulting in the gripping to be combined sets of wrist synergies and additional grip muscle synergy that activate only on the gripping. Such supplementary synergy set cannot split off one specific DOF activity from the EMG signals, interfering wrist joint estimates at the gripping trial. Among the five synergy matrices, Synergy-5 stands for the grip synergy matrix that shows the discrepancy between SLRM1 and SLRM2, and Synergy-5 in SLRM2 contains the co-contraction of the muscles. In time-series synergy coefficients, Synergy 1 to 4 in SLRM1 respond to the grip activation regardless of the force level. The major channels of Synergy-5 are FDS and FDP that are flexor muscles of the finger for gripping from an anatomical aspect. They help to infer grip activation but is insufficient for complex movement estimation. Since grips cause most of the wrist muscle activity, it is essential to identify their co-

contraction ratio for independent estimation. In that sense, the information given in Synergy-5 in SLRM2 played a central role in the complex estimation, the objective of chapter 3.

5.2 The Number of Muscle Synergies in The Trials

In NMF, the synergy number is a parameter that the experimenter must decide. Therefore, it is common to try varying number of synergies. This study also followed 0.9 VAF and 10^{-4} mean squared error when optimizing muscle synergy. Chapter 3 used the same synergy number per trial from the anatomical basis EMG signals. But in chapter 4 where uses high-density EMGs, each participant had different synergy number defined from 0.9 VAF. One consistent factor in the two analyses was that 0.9 VAF gave an optimized performance. The excessive number of synergies increased the classification or linear performance, but that was not enough to show a statistical difference. Mean squared error was applied only in chapter 4, and it converged faster than VAF. It showed that a new threshold is required with a consideration of EMG number. One notable point in the synergy number is that more than 0.9 VAF made the synergy module similar to the actual movement number. The fixed four synergies in chapter 3 were the same number of wrist movements (four perpendicular directions). Chapter 4 gave each different number per participant, but their synergy modules were eight to ten: an approximate number of finger movements. Also, the estimation performance using only the input of these modules were equivalent to the performance from the whole synergies. Though additional verification is demanding, the task constraints may determine the synergy number, not merely influencing the synergy matrix.

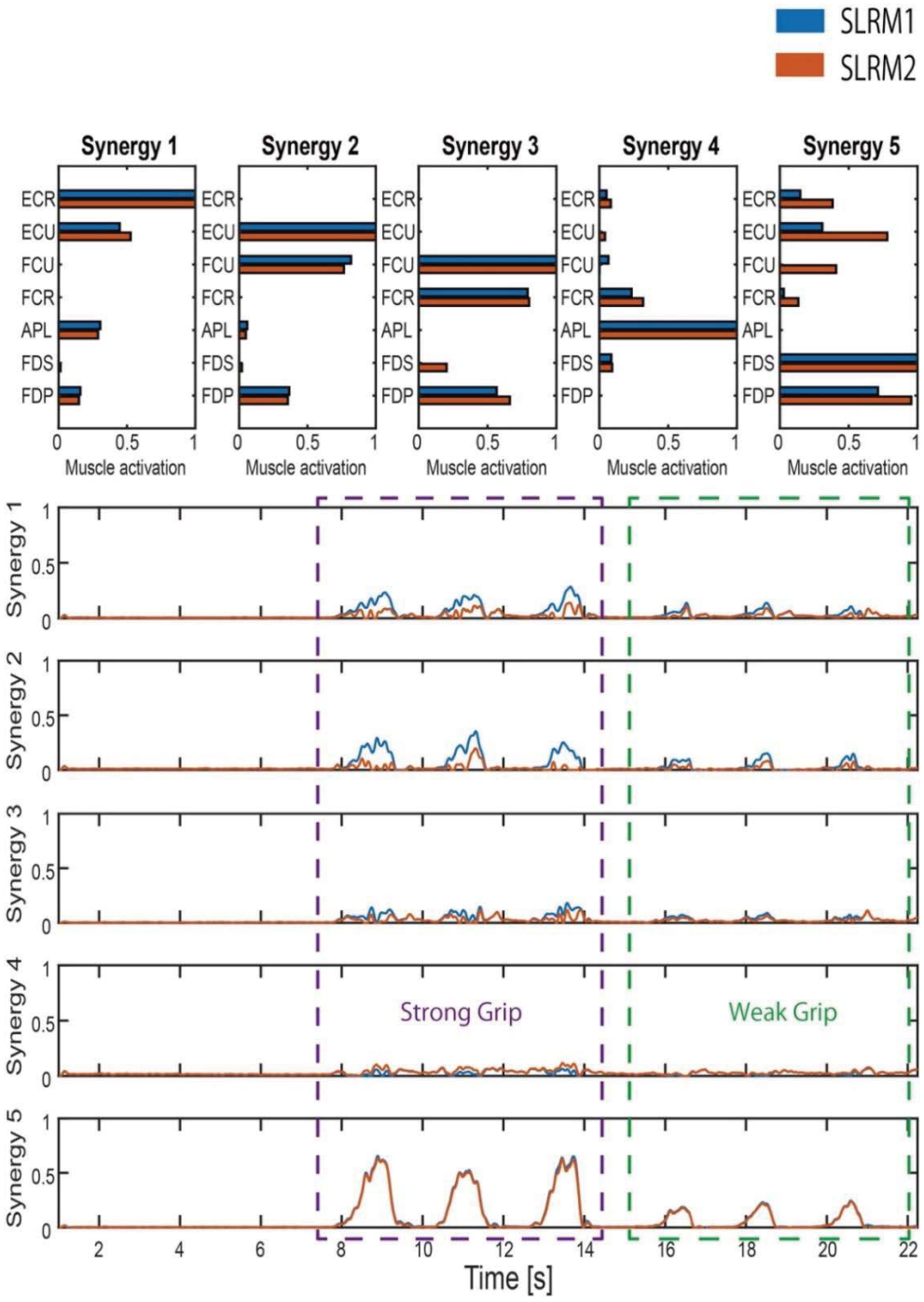

Figure 5.1 Time series synergy coefficient data with corresponding synergy matrix in the synergy-based linear regression model in grip task. Synergies one to four represent wrist synergy, and synergy five represent grip synergy. The purple-colored region represents three times strong grip actions and the green-colored region represents three times weak grip actions.

5.3 The Characteristic of Muscle Synergies and Their Application

As mentioned in the introduction, muscle synergy is defined or hypothesized as a group of muscle activation recruited by a single neural command (Torres-Oviedo, et al., 2006). However, as mentioned in Roh et al., (2012), together with the result section 5.1, the synergy matrix from NMF is task-dependent, affected by task constraints. That task-dependency could change the synergy matrix, converting the resulting synergy matrix the mixture of several neural commands. However, this change could be rather helpful in classifying the input signal. The separate computation combines the multiple neural commands for gripping. Such bindings of synergy model enabled discriminating movement type which can be defined by the training set as depicted in chapter 3.

Muscle synergy could utilize not only NMF but also ICA right after EMG extraction. The sequential combination enabled identifying the deep muscle activity, generally hard to distinguish from the noise components because of their small-signal size. Figure 4.6 shows the signal fidelity improvement before and after ICA by comparing EMG and EMG-synergy and IC-synergy in vertical structure synergy structure (Green colored). The muscle synergy could make high-density EMGs reflect high fidelity deep muscle activity, hard to inspect from individual EMG signal. But then there needs further restriction. Any muscle that is likely to give signals could be considered another independent component in the ICA analysis. This deep muscle discrimination ability of ICA could grasp unknown deep muscle activity irrelevant to the target movements. Thus, high-density EMGs using muscle synergies shall require users to consider numerous undesirable deep muscle activities such as postural activities. The detection of all possible muscle activities would be a keystone toward the muscle synergy-based real-time application.

Chapter 6 Conclusion

6.1 Summary

Complex hand estimation in chapter 3 comprised the two-dimensional wrist joint movement and grasping. There evaluated whether continuous estimation is applicable under the simultaneous activation of wrist/hand muscles on the forearm. The result shows that muscle synergy succeeded in separating EMG signals per movement type with sufficient information. The linear of wrist synergies had a comparable wrist joint movement estimation performance with the musculoskeletal model, and the grip synergy could estimate the dynamic gripping force when the wrist motion halted without impacting wrist motion estimate until certain limit. It infers that muscle synergy-based signal decomposition could elicit mutually independent multi-dimensional movements.

Based on the signal source discrimination of the forearm superficial muscles obtained in Chapter 3, in Chapter 4, the analysis was to determine whether signal separation can catch internal finger muscles. The high-density EMG signal had more noises at the sensor level. Even after pre-processing, the signal quality may be worse than that of the EMG sensors attached on the anatomical basis. Thereby, ICA was applied improving the signal fidelity of internal muscle to that of the superficial by recruiting the motor unit action potentials from the diverse signal compound, and NMF reassembled the muscle signal by taking together the similar ICs which gave no effect in performance. Additionally, for this reason, it seems that the increase in performance may not be as large for the anatomy-based EMG signal.

6.2 Future Works

This study found that multi-dimensional motion prediction is possible through multiple BSSs for EMG, and together with high-density multiple sensors, internal muscle patterns can become transparent. However, further studies are needed to establish robustness in a wide range of usage. In combined wrist joint and grasping movement, the grasping began to affect wrist estimation at a specific power level. The limit is on-demand for further investigation. Also, the dynamic estimation of wrist joint and grasping shall need extra examination. Besides, there are more grip types and activities with fingers. There should be further research focusing on robustness and other restrictions. In a complex movement investigation with a high-density EMG system, current research results are only a stage of proposing possibilities rather than demonstrating a basis. Therefore, it is necessary to investigate whether these research results are valid through research under more diverse conditions.

References

Ameri, A., Akhaee, M. A. & Scheme, E., 2019. Regression convolutional neural network for improved simultaneous EMG control. *Journal of Neural Engineering,* 16(3), p. 036015.

Antuvan, C. W. et al., 2016. Role of muscle synergies in real-time classification of upper limb motions using extreme learning machines. *Journal of Neuroengineering and Rehabilitation,* 13(1), p. 76.

Artemiadis, P. K. & Kyriakopoulos, K. J., 2010. A switching regime model for the EMG-based control of a robot arm. *IEEE Transactions on Systems, Man, and Cybernetics, Part B (Cybernetics),* 41(1), pp. 53-63.

Bernstein, N., 1967. *The co-ordination and regulation of movements.*. University of California: Pergamon-Press.

Biddiss, E., 2009. Need-Directed Design of Prostheses and Enabling Resources. In: *Amputation, Prosthesis Use, and Phantom Limb Pain.* New York: Springer, pp. 7-21.

Blanc, Y. & Dimanico, U., 2010. Electrode placement in surface electromyography (sEMG)" Minimal Crosstalk Area "(MCA). *The Open Rehabilitation Journal,* 3(1).

Castellini, C. & Van, P. D. S., 2009. Surface EMG in advanced hand prosthetics. *Biological cybernetics,* 100(1), pp. 35-47.

Cheung, V. C., d'Avella, A., Tresch, M. C. & Bizzi, E., 2005. Central and sensory contributions to the activation and organization of muscle synergies during natural motor behaviors. *Journal of Neuroscience,* 25(27), pp. 6419-6434.

Cheung, V. C. et al., 2012. Muscle synergy patterns as physiological markers of motor cortical damage. *Proceedings of the national academy of sciences,* 109(36), pp. 14652-14656.

Chowdhury, R. H. et al., 2013. Surface electromyography signal processing and classification techniques. *Sensors,* 13(9), pp. 12431-12466.

Cichocki, A. & Phan, A.-H., 2009. Fast Local Algorithms for Large Scale Nonnegative Matrix and Tensor Factorizations. *IEICE TRANSACTIONS on Fundamentals of Electronics, Communications and Computer Sciences,* 92(3), pp. 708-721.

Clancy, E. A. & Hogan, N., 1995. Multiple site electromyograph amplitude estimation. *IEEE Transactions on Biomedical Engineering,* 42(2), pp. 203-211.

Clark, D. J. et al., 2010. Merging of healthy motor modules predicts reduced locomotor performance and muscle coordination complexity post-stroke. *Journal of neurophysiology,* 103(2), pp. 844-857.

d'Avella, A., Portone, A., Fernandez, L. & Lacquaniti, F., 2006. Control of fast-reaching movements by muscle synergy combinations. *Journal of Neuroscience,* 26(30), pp. 7791-7810.

De Luca, C. J., Gilmore, L. D., Kuznetsov, M. & Roy, S. H., 2010. Filtering the surface EMG signal: Movement artifact and baseline noise contamination. *Journal of biomechanics,* 43(8), pp. 1573-1579.

Furui, A. et al., 2019. A myoelectric prosthetic hand with muscle synergy–based motion determination and impedance model–based biomimetic control. *Science Robotics,* 4(31).

Gazzoni, M. et al., 2014. Quantifying forearm muscle activity during wrist and finger movements by means of multi-channel electromyography. *PloS one,* 9(10), p. e109943.

Gentner, R., Edmunds, T., Pai, D. K. & d'Avella, A., 2013. Robustness of muscle synergies during visuomotor adaptation. *Frontiers in computational neuroscience,* Volume 7, p. 120.

Halaki, M. & Ginn, K., 2012. Normalization of EMG signals: to normalize or not to normalize and what to normalize to.. In: *Computational Intelligence in Electromyography Analysis.* s.l.:s.n., pp. 175-194.

Hooda, N., Das, R. & Kumar, N., 2020. Fusion of EEG and EMG signals for classification of unilateral foot movements.. *Biomedical Signal Processing and Control,* Volume 60, p. 101990.

Hyvärinen, A. & Oja, E., 2000. "Independent component analysis: algorithms and applications. *Neural networks,* 13(4-5), pp. 411-430.

Ison, M. & Artemiadis, P., 2015. Proportional myoelectric control of robots: muscle synergy development drives performance enhancement, retainment, and generalization. *IEEE Transaction on Robotics,* 31(2), pp. 259-268.

Jiang, N., Vest-Nielsen, J. L., Muceli, S. & Farina, D., 2012. EMG-based simultaneous and proportional estimation of wrist/hand kinematics in uni-lateral trans-radial amputees. *Journal of neuroengineering and rehabilitation,* 9(1), pp. 1-11.

Jung, T. et al., 2000. Removing electroencephalographic artifacts by blind source separation. *Psychophysiology,* 37(2), pp. 163-178.

Kambara, H., Shin, D. & Koike, Y., 2013. A computational model for optimal muscle activity considering muscle viscoelasticity in wrist movements. *Journal of neurophysiology,* 109(8), pp. 2145-2160.

Kawase, T., Sakurada, T., Koike, Y. & Kansaku, K., 2017. A hybrid BMI-based exoskeleton for paresis: EMG control for assisting arm movements. *Journal of Neural Engineering,* 14(1), p. 016015.

Keen, D. A. & Fuglevand, A. J., 2004. Distribution of motor unit force in human extensor digitorum assessed by spike-triggered averaging and intraneural microstimulation. *Journal of neurophysiology,* 91(6), pp. 2515-2523.

Khokhar, Z. O., Xiao, Z. G. & Menon, C., 2010. Surface EMG pattern recognition for real-time control of a wrist exoskeleton. *Biomedical engineering online,* 9(1), pp. 1-17.

Kita, K., Kato, R., Yokoi, H. & Arai, T., 2006. *Development of autonomous assistive devices-analysis of change of human motion patterns.* Taipei, IEEE, pp. 316-321.

Koike, Y. & Kawato, M., 1995. Estimation of dynamic joint torques and trajectory formation from surface electromyography signals using a neural network model. *Biological Cybernetics,* 73(4), pp. 291-300.

Kothe, C., 2014. *Lab streaming layer (LSL).* [Online]
Available at: https://github. com/sccn/labstreaminglayer
[Accessed 26 October 2015].

Krizhevsky, A., Sutskever, I. & Hinton, G. E., 2012. Imagenet classification with deep convolutional neural networks. *Advances in neural information processing systems,* Volume 25, pp. 1097-1105.

Lee, D. D. & Seung, H. S., 2001. *Algorithms for non-negative matrix factorization.* Denver, Neural information processing systems foundation.

Lee, J., Kagamihara, Y. & Kakei, S., 2015. A new method for functional evaluation of motor commands in patients with cerebellar ataxia. *PloS one,* 10(7), p. e0132983.

Madgwick, S., 2010. *An efficient orientation filter for inertial and inertial/magnetic sensor arrays,* Bristol: Report x-io.

Matsunaga, N., Imai, A. & Kaneoka, K., 2017. Comparison of muscle synergies before and after 10 minutes of running. *Journal of physical therapy science,* 29(7), pp. 1242-1246.

Mukhopadhyay, A. K. & Samui, S., 2020. An experimental study on upper limb position invariant EMG signal classification based on deep neural network. *Biomedical Signal Processing and Control,* Volume 55, p. 101669.

Nei, M. & Kumar, S., 2000. Phylogenetic Inference: Distance Methods. In: *Molecular Evolution and Phylogenetics.* s.l.:Oxford university press, pp. 87-92.

Nielsen, J. L. et al., 2010. Simultaneous and proportional force estimation for multifunction myoelectric prostheses using mirrored bilateral training. *IEEE Transactions on Biomedical Engineering,* 58(3), pp. 681-688.

Nishikawa, D., Yu, W., Yokoi, H. & Kakazu, Y., 1999. *EMG prosthetic hand controller using real-time learning method.* Tokyo, IEEE, pp. 153-158.

Phinyomark, A. N., Khushaba, R. & Scheme, E., 2018. Feature extraction and selection for myoelectric control based on wearable EMG sensors. *Sensors,* 18(5), p. 1615.

Roh, J., Rymer, W. Z. & Beer, R. F., 2012. Robustness of muscle synergies underlying three-dimensional force generation at the hand in healthy humans. *Journal of neurophysiology,* 107(8), pp. 2123-2142.

Santuz, A. et al., 2017. On the methodological implications of extracting muscle synergies from human locomotion. *International journal of neural systems,* 27(5), p. 1750007.

Schieber, M. H., 1995. Muscular production of individuated finger movements: the roles of extrinsic finger muscles. *Journal of Neuroscience,* 15(1), pp. 284-297.

Sebelius, F. et al., 2005. Real-time control of a virtual hand. *Technology and Disability,* 17(3), pp. 131-141.

Shima, K. & Tsuji, T., 2010. Classification of combined motions in human joints through learning of individual motions based on muscle synergy theory.. *2010 IEEE/SICE International Symposium on System Integration*, pp. 323-328.

Simão, M., Neto, P. & Gibaru, O., 2019. EMG-based online classification of gestures with recurrent neural networks. *Pattern Recognition Letters,* Volume 128, pp. 45-51.

Staudenmann, D. et al., 2007. Independent component analysis of high-density electromyography in muscle force estimation. *IEEE transactions on biomedical engineering,* 54(4), pp. 751-754.

Staudenmann, D. et al., 2006. Improving EMG-based muscle force estimation by using a high-density EMG grid and principal component analysis. *IEEE Transactions on Biomedical Engineering,* 53(4), pp. 712-719.

Ting, L. H. & McKay, J. L., 2007. Neuromechanics of muscle synergies for posture and movement. *Current opinion in neurbiology,* 17(6), pp. 622-628.

Torres-Oviedo, G., Macpherson, J. M. & Ting, L. H., 2006. Muscle synergy organization is robust across a variety of postural perturbations. *Journal of Neurophysiology,* 96(3), pp. 1530-1546.

Tresch, M. C., Saltiel, P. & Bizzi, E., 1999. The construction of movement by the spinal cord. *Nature Neuroscience,* 2(2), pp. 162-167.

Xia, P., Hu, J. & Peng, Y., 2018. EMG-based estimation of limb movement using deep learning with recurrent convolutional neural networks. *Artificial organs,* 42(5), pp. E66-E77.

Yeong, C. F., Melendez-Calderon, A., Gassert, R. & Burdet, E., 2009. *ReachMAN: a personal robot to train reaching and manipulation.* St. Louis, IEEE, pp. 4080-4085.

Yoshimura, N. et al., 2017. Decoding finger movement in humans using synergy of EEG cortical current signals. *Scientific reports,* 7(1), pp. 1-11.

Publication Related to This Study

Kim, Y. et al., 2020. Muscle synergy and musculoskeletal model-based continuous multi-dimensional estimation of wrist and hand motions. *Journal of healthcare engineering*, 2020

Kim, Y. et al., 2020. The Effect of ICA and Non-negative Matrix Factorization Analysis for EMG Signals Recorded From Multi-Channel EMG Sensors. *Frontier in Neuroscience*, 14, pp. 1254